iScience

CellPress
OPEN ACCESS

Article

AKT2-mediated nuclear deformation leads to genome instability during epithelial-mesenchymal transition

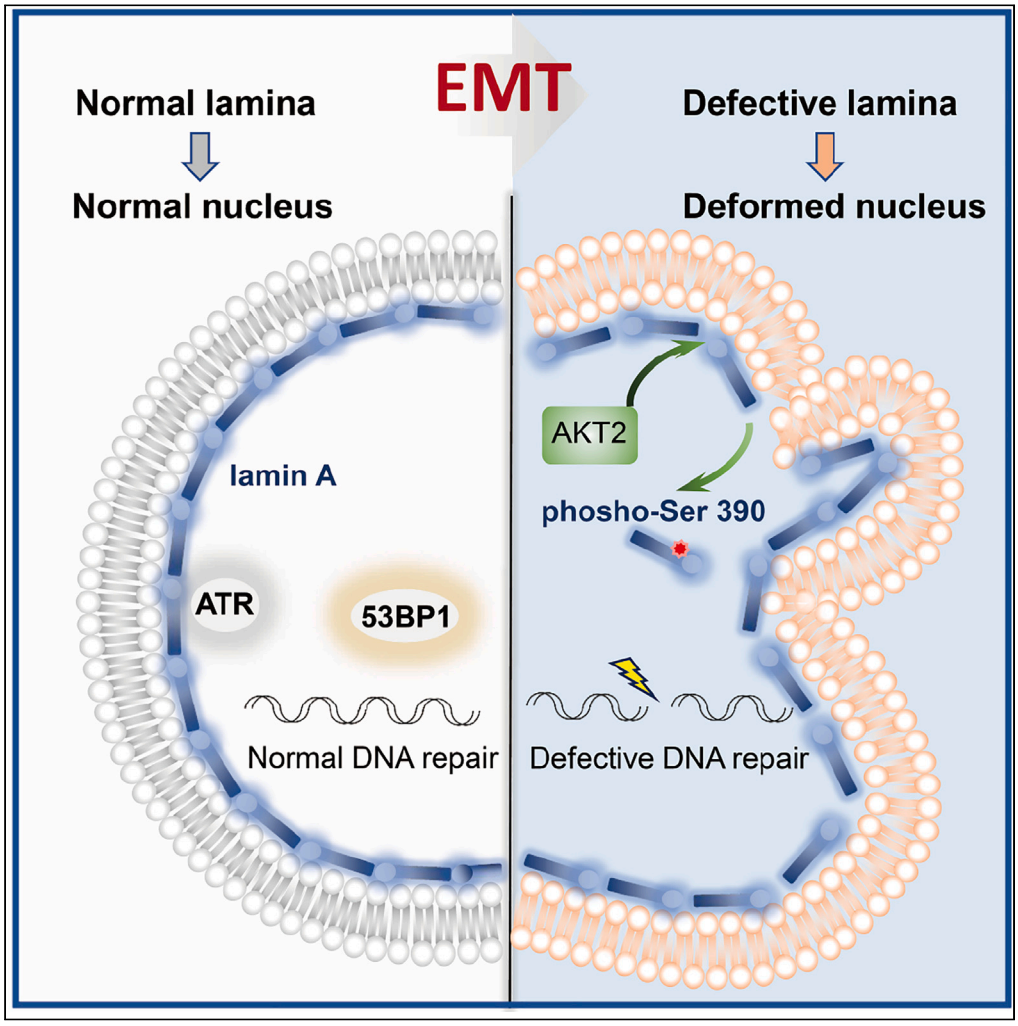

Jia-Rong Fan, Sung-Nian Chang, Ching-Tung Chu, Hong-Chen Chen

hcchen1029@nycu.edu.tw

Highlights

AKT2 phosphorylates lamin A at S390 on TGFβ stimulation

Phosphorylation of lamin A at S390 contributes to nuclear deformation during EMT

The DNA repair proteins ATR and 53BP1 become defective in deformed nuclei

Nuclear deformation is tightly associated with genome instability during EMT

Fan et al., iScience 26, 106992
June 16, 2023
https://doi.org/10.1016/j.isci.2023.106992

iScience

CellPress
OPEN ACCESS

Article

AKT2-mediated nuclear deformation leads to genome instability during epithelial-mesenchymal transition

Jia-Rong Fan,[1,2] Sung-Nian Chang,[1] Ching-Tung Chu,[1] and Hong-Chen Chen[1,2,3,*]

SUMMARY

Nuclear deformation has been observed in some cancer cells for decades, but its underlying mechanism and biological significance remain elusive. To address these questions, we employed human lung cancer A549 cell line as a model in context with transforming growth factor β (TGFβ)-induced epithelial-mesenchymal transition. Here, we report that nuclear deformation induced by TGFβ is concomitant with increased phosphorylation of lamin A at Ser390, defective nuclear lamina and genome instability. AKT2 and Smad3 serve as the downstream effectors for TGFβ to induce nuclear deformation. AKT2 directly phosphorylates lamin A at Ser390, whereas Smad3 is required for AKT2 activation upon TGFβ stimulation. Expression of the lamin A mutant with a substitution of Ser390 to Ala or suppression of AKT2 or Smad3 prevents nuclear deformation and genome instability induced by TGFβ. These findings reveal a molecular mechanism for TGFβ-induced nuclear deformation and establish a role of nuclear deformation in genome instability during epithelial-mesenchymal transition.

INTRODUCTION

Epithelial-mesenchymal transition (EMT), a process that epithelial cells lose their polarity and gain migratory and invasive properties to become mesenchymal stem cells, is essential for development, wound healing, and cancer progression.[1] EMT enables tumor cells to not only gain a migratory phenotype but induce multiple mechanisms toward to immunosuppression, drug resistance, and evasion of apoptosis.[1] The characteristics of cells that undergo EMT include loss of cell-cell junctions, mesenchymal morphological changes, increased extracellular matrix expression, elevated migratory and invasive properties, nuclear deformation, and genome instability.[2–4] Genome instability has been regarded as the initiation of tumorigenesis.[5] Nuclear deformation or dysmorphia, characterized by crumpled or lobulated polymorphic nuclear shapes, has been applied to clinical diagnosis for the malignant grades of certain cancers.[6–8]

EMT can be induced by several growth factors and cytokines (e.g., TGFβ, FGF, EGF, HGF, Wnt/β-catenin and Notch) as well as hypoxia.[4,9] Among which, transforming growth factor β (TGFβ) is prominent for its capability to induce EMT in various *in vitro* models.[10,11] On binding to its receptor, TGFβ triggers the activation of the Smad and non-Smad signaling pathways.[4] Most of the TGFβ-induced transcriptional responses are mediated by Smad2 and Smad3, both of which are members of the receptor-regulated Smad (R-Smad) family.[12] On phosphorylated by the TGFβ-receptor, Smad2/3 bind to the Co-Smad Smad4 and then the R-Smad/Co-Smad complexes translocate into the nucleus where they cooperate with context-specific transcription factors to regulate target gene expression.[13] Although Smad2 and Smad3 share common functions, increasing evidence indicates that they can perform distinct functions.[14–16] Besides activation of the canonical Smad pathway, TGFβ also modulates the activity of several other signaling pathways, such as the Ras-MAPK (Mitogen-Activated Protein Kinase) and phosphatidylinositol 3-kinase (PI3K)-AKT signaling pathways.[17] Unlike the canonical Smad pathway, modulation of these non-Smad pathways by TGFβ is often cell type-specific and context-dependent.[17] In mammalian cells, all three MAPKs (i.e., Erk, Jnk, and p38) are activated by TGFβ.[18–20] The TGFβ-stimulated Erk activation is crucial for specific induction of genes that feature prominently in cell motility and cell-matrix interaction,[21] while the PI3K-AKT signaling pathway contribute to E-cadherin repression and invasive behavior during EMT.[22–26]

The mammalian AKT family includes three closely related serine/threonine protein kinases (AKT1, AKT2, and AKT3), which regulate many processes including metabolism, proliferation, cell survival, growth,

[1]Institute of Biochemistry and Molecular Biology, National Yang Ming Chiao Tung University, Taipei 11221, Taiwan

[2]Cancer Progression Research Center, National Yang Ming Chiao Tung University, Taipei 11221, Taiwan

[3]Lead contact

*Correspondence: hcchen1029@nycu.edu.tw

https://doi.org/10.1016/j.isci.2023.106992

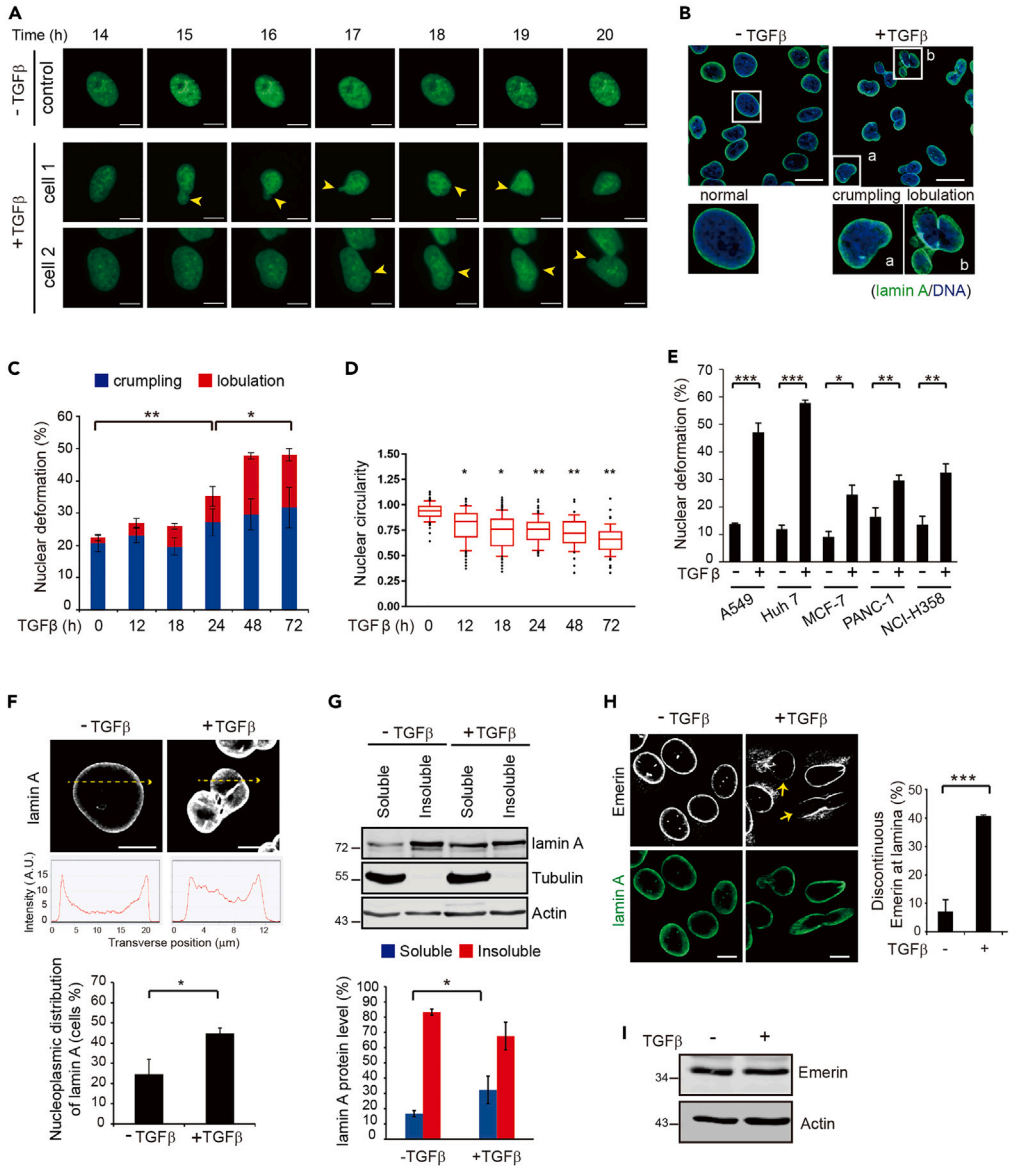

Figure 1. TGFβ induces nuclear deformation, concomitant with defective nuclear lamina

(A) Representative time-lapse images of A549 cells expressing GFP-H2B in the presence (+) or absence (–) of TGFβ are shown. The alteration in the nuclear morphology became more evident 15 h after TGFβ stimulation. The arrowheads indicate irregular nuclear shapes. Scale bars, 10 μm.

(B) A549 cells were treated with (+) or without (–) TGFβ for 72 h and stained for lamin A (green) and DNA (blue). The insets show a normal nucleus and two deformed nuclei classified as crumpling (**a**) or lobulation (**b**). Scale bars, 20 μm.

(C) A549 cells were treated with TGFβ for various times as indicated and stained for lamin A and DNA. The percentage of the cells with a crumpled or lobulated nucleus was measured ($n \geq 339$).

(D) A549 cells were treated with TGFβ for various times as indicated and stained for lamin A and DNA. The nuclear circularity (4π x area/perimeter^2) of the cells was determined ($n \geq 100$).

(E) Various cancer cell lines, as indicated, were treated with TGFβ for 72 h and stained for lamin A and DNA. The percentage of the cells with a deformed nucleus was measured ($n \geq 600$).

(F) A549 cells were treated with or without TGFβ for 72 h and stained for lamin A. The line-scan profiles of lamin A at the selected region (as indicated by dashed lines) are shown using Zeiss Zen2 software. Scale bars, 10 μm. The percentage of the cells with apparent nucleoplasmic distribution of lamin A was measured ($n \geq 246$).

(G) A549 cells were treated with or without TGFβ for 72 h and solubilized in 1% NP40 lysis buffer. An equal proportion of cell lysates from the soluble and insoluble fractions was analyzed by immunoblotting with the antibodies as indicated. The

Figure 1. *Continued*

level of lamin A in the soluble and insoluble fractions was quantified and expressed as the percentage of each fraction in the total counts.

(H) A549 cells were treated with or without TGFβ for 72 h and stained for emerin (white), lamin A (green), and DNA (blue). The arrows indicate the region of the nuclear lamina without emerin distribution. Scale bars, 10 μm. The percentage of the cells with a discontinuous distribution of emerin at the nuclear lamina was measured ($n \geq 200$).

(I) A549 cells were treated with or without TGFβ for 72 h and lysed. An equal amount of whole cell lysates was analyzed by the immunoblotting with anti-emerin or anti-actin antibody. Data information: In C, E, F, G and H, values (means ± SD) were from three independent experiments. In D, values were presented as the box-whisker plot from three independent experiments. *$p < 0.05$, **$p < 0.01$, ***$p < 0.001$. See also Figure S1.

and angiogenesis.[27] AKT1 and AKT2 are ubiquitously expressed in most tissues, whereas AKT3 appears to be predominantly expressed in brain.[28,29] Because of strong homologies in the primary amino acid sequence, the three AKT isoforms were long surmised to play redundant and overlapping roles. However, more and more studies have pointed to isoform specific functions in different cellular events and diseases.[30] For example, AKT1 is more specifically involved in cell growth and survival,[31,32] whereas AKT2 is more specific for cancer metastasis.[33–35] In addition, AKT2 has been found to be upregulated, mutated, and correlated with poor prognosis in several types of cancers.[34,36,37]

The nuclear lamina is a dense fibrillar network that is composed of lamins (type V intermediate filament proteins) and nuclear membrane-associated proteins. It associates with the inner nuclear membrane of the nuclear envelope and thereby provides mechanical strength to the nucleus. In addition, the nuclear lamina participates in chromatin organization and regulates various important nuclear activities including transcription, DNA replication, and DNA damage repair, which occur through interaction with chromatins and signaling proteins.[38,39] The genomes of mammals have three lamin genes: *LMNA, LMNB1,* and *LMNB2*. The *LMNA* gene is expressed in differentiated cells, whereas at least one *LMNB* gene is expressed in every somatic cell in the body.[40,41] Lamins were found to be phosphorylated at serine and tyrosine residues during interphase and mitosis.[42–46] In most cases, phosphorylation of lamins has an adverse effect on their assembly. Lamin A is most studied among lamins. It is a heavily phosphorylated protein with more than 70 identified unique Ser/Thr phosphorylation sites,[47,48] some of which (Ser22, Ser390, Ser392, and Ser404) have been shown to affect the structure and function of lamin A during interphase and mitosis.[46] More recently, Src was found to phosphorylate lamin A mainly at Tyr45, which hampers lamin A assembly in the interphase.[42] Besides phosphorylation, SUMOylation and acetylation of lamin A were reported to be important for maintaining nuclear architecture and genome integrity.[49,50]

Nuclear deformation is usually accompanied by loss of the nuclear envelope integrity, aberrant gene expression, and genome instability.[51] All of these relevant events can be observed not only in malignant tumor cells, but also in the cells derived from patients with laminopathies, a group of rare genetic disorders caused by mutations in the *LMNA* gene.[52–54] Likewise, down-regulation of lamin A was able to cause nuclear deformation in lung and breast cancer cells.[55,56] Lamin A has been reported to be involved in the DNA damage response partly through ensuring proper nuclear localization and/or expression of DNA repair proteins, including 53BP1, ATR, DNA-PK, Rad51, and BRCA1.[57–63] Therefore, nuclear deformation caused by lamin A deficiency may impair the DNA repair mechanism and lead to genome instability. Besides, under certain circumstances, post-translational modification of lamin A that alters the structure of the nuclear lamina may cause nuclear deformation and genome instability. It was reported that deficiency of nestin (a biomarker for stem cells) caused lamin A phosphorylation mainly at Ser392 by CDK5, which induced lamin A degradation and nuclear deformation, in association with tumor senescence.[64] Although there has been increasing attention paid to nuclear deformation, the underlying mechanism and its biological significance during EMT are still elusive. In the present study, we show that nuclear deformation induced by TGFβ is concomitant with increased lamin A phosphorylation mainly at Ser390, defective nuclear lamina, and genome instability. Our mechanistic study reveals that AKT2 and Smad3 are the downstream effectors for TGFβ to induce such events.

RESULTS

TGFβ induces nuclear deformation, accompanied by defective nuclear lamina

The human lung cancer A549 cell line has been widely used as a model to study TGFβ-induced EMT.[65–67] In this study, we observed that A549 cells constantly changed their nuclear shape and apparently exhibited irregular deformed nuclei 15 h after TGFβ treatment (Figure 1A). The nuclear deformation induced by

TGFβ can be classified as crumpling (mildly deformed) or lobulation (severely deformed) by immunofluorescence staining with anti-lamin A (Figure 1B, and see STAR Methods for the criteria). The deformed nuclei of A549 cells arose from ~22% (mainly crumpled nuclei) at 0 h to ~35% at 24 h, and up to ~48% (approximately one-third of which were lobulated nuclei) at 48 h after TGFβ treatment (Figure 1C). Accordingly, the nuclear circularity (4πx area/perimeter^2) of the cells were gradually decreased from 0.8 at 0 h to 0.55 at 72 h of TGFβ treatment (Figure 1D). In addition to A549 cells, TGFβ has been reported to induce EMT in liver cancer Huh7 cells, breast cancer MCF7 cells, pancreatic cancer PANC1 cells, and lung cancer NCI-H358 cells.[68–71] Indeed, TGFβ also induced nuclear deformation in those cell lines with various extents (Figure 1E). Moreover, although EGF and HGF have been reported to induce EMT,[4,9] both of which induced neither EMT nor nuclear deformation in A549 cells (Figure S1). These results together implicate that the capability of TGFβ to induce nuclear deformation seemingly associate with its potential to induce EMT.

The involvement of the nuclear lamina in the TGFβ-induced nuclear deformation was examined. We found that the deformed nucleus had an increased level of lamin A in the nucleoplasm, as shown by the transverse line-scan of microscopy (Figure 1F). In addition, lamin A became more soluble after TGFβ treatment, as revealed by increased NP40-extractable lamin A (the soluble fraction in Figure 1G). The distribution of emerin, a lamin A-interacting protein, at the nuclear lamina has been used as a marker for the integrity of the nuclear lamina.[72,73] We found that emerin discontinuously distributed at the nuclear lamina of deformed nuclei (Figure 1H). This discontinuity of emerin at the nuclear lamina was not attributed to decreased protein expression of emerin (Figure 1I). These data indicate that the nuclear deformation induced by TGFβ is associated with defective nuclear lamina.

The phosphorylation of lamin A at Ser390 is important for TGFβ to induce nuclear deformation

It has been shown that phosphorylation of lamin A at specific serine residues modulates the assembly of the nuclear lamina in both interphase[44,46] and mitotic phase.[43,45] We found that lamin A phosphorylation at Ser390 (pS390) was increased up to 2.8-fold at 72 h after TGFβ treatment, whereas other lamin A phosphorylation sites, including Ser22, Ser392, and Ser404, were not evidently enhanced (Figure 2A). The increased lamin A pS390 was concomitant with appearance of EMT markers, including a decreased expression of E-cadherin and increased levels of vimentin, Slug, and Twist (Figure 2A). To examine whether the phosphorylation of lamin A at Ser390 is important for TGFβ-induced nuclear deformation, lamin A mutants with a substitution at Ser22, Ser390, Ser392 or Ser404 were transiently expressed in A549 cells (Figure 2B). We found that among the mutants, the S390A mutant showed the most resistance to nuclear deformation induced by TGFβ (Figure 2C). These data suggest that the phosphorylation of lamin A at S390 may be a prerequisite for nuclear deformation on TGFβ stimulation.

AKT2, but not AKT1, is responsible for lamin A phosphorylation at Ser390 on TGFβ stimulation

To explore which kinase(s) is responsible for TGFβ-induced lamin A pS390 and nuclear deformation, A549 cells were treated with pharmacological inhibitors for the kinases (AKT, ERK, JNK, and p38) that were reported to engage in TGFβ-induced EMT.[74] Among these inhibitors, only the AKT-specific inhibitor MK2206 prominently suppressed TGFβ-induced nuclear deformation in a dose-dependent manner (Figure 3A). AKT isozymes, AKT1 and AKT2, were activated on TGFβ stimulation, both of which were inhibited by MK2206 (Figure S2A). The inhibition of nuclear deformation by MK2206 also restored the nuclear lamina, as revealed by well distribution of lamin A and emerin at the nuclear lamina (Figures S2B and S2C). Accordingly, the inhibitor LY294002 specific to PI3K, the upstream activator of AKT, significantly suppressed TGFβ-induced nuclear deformation (Figure 3B).

The inhibition of AKT by MK2206 diminished ~52% of lamin A pS390 induced by TGFβ (Figure 3C). To examine which AKT isozyme is responsible for TGFβ-induced lamin A pS390 and nuclear deformation, AKT1 and AKT2 were respectively depleted by specific shRNAs. Surprisingly, the depletion of AKT2, but not AKT1, suppressed lamin A pS390 (Figure 3D) and nuclear deformation (Figure 3E) on TGFβ stimulation. Moreover, overexpression of exogenous HA-AKT2, but not HA-AKT1, was sufficient to induce nuclear deformation, even in the absence of TGFβ stimulation (Figures 3F and S2D).

To examine whether lamin A Ser390 was preferentially phosphorylated by AKT2 rather than AKT1 in intact cells, HA-AKT1 and HA-AKT2 were transiently overexpressed in 293T cells. The total lamin A

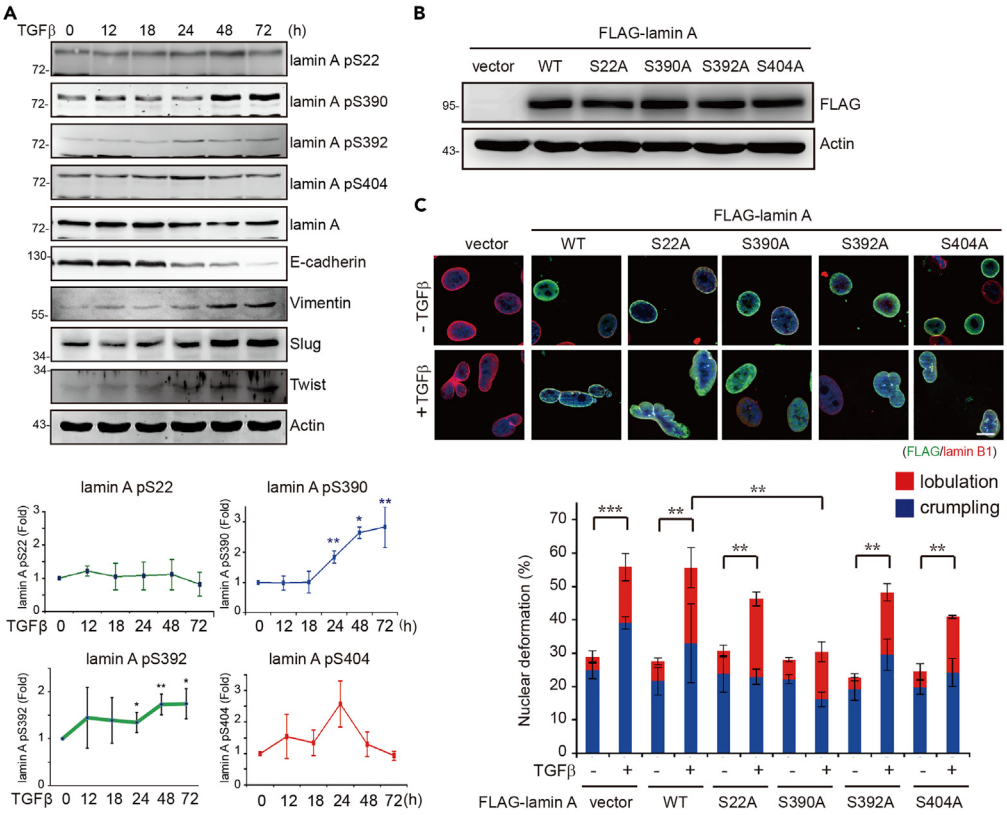

Figure 2. TGFβ increases lamin A phosphorylation mainly at Ser390, which is essential for TGFβ-induced nuclear deformation

(A) A549 cells were treated with TGFβ for various times as indicated and analyzed by immunoblotting with the antibodies as indicated. The phosphorylation levels of lamin A at Ser22, Ser390, Ser392, and Ser404 were quantified and expressed as -fold relative to the level at time 0.

(B) FLAG-lamin A wild type (WT) or the mutants as indicated were transiently expressed in A549 cells for 24 h. An equal amount of whole cell lysates was analyzed by immunoblotting with anti-FLAG or anti-actin antibody.

(C) A549 cells transiently expressing FLAG-lamin A or the mutants were treated with TGFβ for 72 h and stained for FLAG-lamin A (green), lamin B1 (red), and DNA (blue). Scale bars, 10 μm. The percentage of the transfection-positive cells with a crumpled or lobulated nucleus was measured (n ≥ 288). Data information: In A and C, values (means ± SD) were from three independent experiments. **p < 0.01, ***p < 0.001.

phosphorylation (as visualized by staining the gel with Phos-Tag) and lamin A pS390 level (as visualized by immunoblotting with anti-lamin A pS390) were remarkably elevated by HA-AKT2, but only slightly increased by HA-AKT1 (Figure 3G). The capability of HA-AKT2 to increase lamin A pS390 was ~4.6-fold of HA-AKT1, as measured by lamin A pS390 intensity/HA-AKT intensity. The results from the *in vitro* kinase assay clearly showed that AKT2, but not AKT1, directly phosphorylated lamin A at Ser390 (Figure 3H). Of interest, both AKT isozymes phosphorylated lamin A at Ser404 to similar extent, but neither one phosphorylated lamin A at Ser22 (Figure 3H). Together, these results indicate that AKT2 is the key kinase responsible for lamin A Ser390 as well as nuclear deformation on TGFβ stimulation.

Smad3 facilitates AKT2 activation and thereby contributes to nuclear deformation on TGFβ stimulation

To examine whether the Smad signaling is involved in TGFβ-nuclear deformation in in A549 cells, Smad2 and Smad3 were respectively depleted by specific shRNAs (Figure 4A). We found that the depletion of Smad3, but not Smad2, suppressed TGFβ-induced nuclear deformation (Figure 4B). On the other hand, overexpression of Smad3 by itself caused nuclear deformation, yet Smad2 had no such an effect (Figure 4C). Moreover, we found that suppression of Smad3 by shRNA or the specific inhibitor SIS3[75] inhibited TGFβ-induced phosphorylation of AKT2 at Ser474 (Figures 4D and 4E). These data suggest that Smad3 may

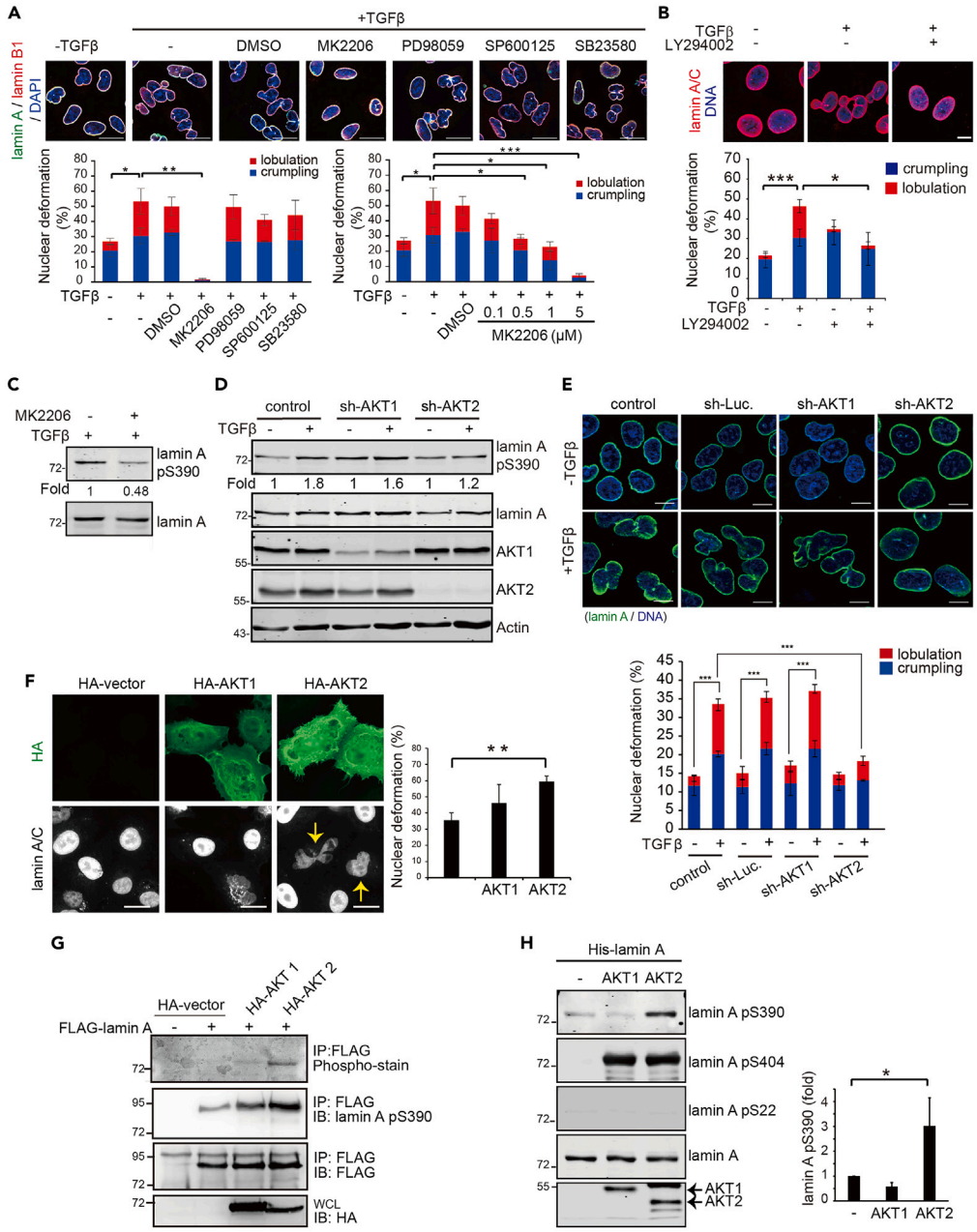

Figure 3. AKT2 is responsible for lamin A Ser390 phosphorylation and nuclear deformation on TGFβ stimulation

(A) A549 cells were pre-treated with MK2206 (AKT inhibitor; 5 μM), PD98059 (ERK inhibitor; 20 μM), SP600125 (JNK inhibitor; 10 μM), SB23580 (p38 inhibitor; 10 μM), or the solvent DMSO as the control for 1 h and then co-treated with TGFβ for 72 h. The cells were stained for lamin A (green), lamin B1 (red), and DNA (blue). Representative images are shown. Scale bars, 20 μm. The percentage of the cells with a crumpled or lobulated nucleus was measured (n = 300). To further confirm the inhibitory effect of MK2206 on TGFβ-induced nuclear deformation, A549 cells were treated with TGFβ in the presence of MK2206 at various concentrations as indicated for 72 h. The percentage of the cells with a crumpled or lobulated nucleus was measured (n = 300).

(B) A549 cells were pre-treated with LY294002 (PI3K inhibitor; 20 μM) for 1 h and then co-treated with TGFβ for 72 h. The cells were stained for lamin A (red) and DNA (blue). Representative images are shown. Scale bars, 10 μm. The percentage of the cells with a crumpled or lobulated nucleus was measured (n ≥ 245).

(C) A549 cells were pre-treated with or without MK2206 (5 μM) for 1 h and co-treated with TGFβ for 48 h. The cells were lysed and an equal amount of whole cell lysates was analyzed by immunoblotting with anti-lamin A or anti-lamin A pS390

Figure 3. *Continued*

antibody. The level of lamin A pS390 was measured and expressed as -fold relative to the level of the cells without MK2206 treatment.

(D) A549 cells were infected with lentiviruses encoding shRNAs specific to AKT1 (sh-AKT1) or AKT2 (sh-AKT2). The cells were treated with TGFβ for 72 h and lysed. An equal amount of whole cell lysates was analyzed by immunoblotting with the antibodies as indicated. The level of lamin A pS390 was measured and expressed as -fold relative to the level of the control group without TGFβ treatment.

(E) A549 cells as described in (D) were treated with TGFβ for 24 h and stained for lamin A (green) and DNA (blue). Representative images are shown. Scale bars, 10 μm. The percentage of the cells with a crumpled or lobulated nucleus was measured ($n \geq 600$).

(F) A549 cells were transiently transfected with the plasmid encoding HA-AKT1 or HA-AKT2 for 24 h and then stained for HA-AKT (green) and lamin A (white). The arrows indicate deformed nuclei. Scale bars, 20 μm. The percentage of the transfection-positive cells with a deformed nucleus was measured ($n \geq 457$).

(G) FLAG-lamin A was transiently co-expressed with HA-AKT1 or HA-AKT2 in HEK293T cells for 24 h. The cells were lysed and FLAG-lamin A was immunoprecipitated (IP) from an equal amount of whole cell lysates with anti-FLAG antibody. The immunocomplexes were fractionated by SDS-polyacrylamide gel electrophoresis and the gel was stained with Phos-Tag phosphoprotein gel stain, according to the manufacturer's instructions. Besides, the immunocomplexes were analyzed by immunoblotting with the antibodies as indicated.

(H) Recombinant His-lamin A proteins prepared in our laboratory as described in Materials and Methods were subjected to an *in vitro* kinase assay in the presence of purified recombinant active AKT1 or AKT2 from Merck Millipore. The kinase reaction was terminated with the SDS sample buffer and the proteins in the reaction were analyzed by immunoblotting with the antibodies as indicated. The phosphorylation of His-lamin A at Ser390 was measured and expressed as –fold relative to the level of the control without AKT. Data information: In A, B, E, F and H, values (means ± SD) were from three independent experiments. *$p < 0.05$, **$p < 0.01$, ***$p < 0.001$. See also Figure S2.

facilitate AKT2 activation on TGFβ stimulation. Conversely, the phosphorylation and nuclear translocation of Smad3 was not affected by AKT inhibition (Figure S3).

F-actin and heterochromatin contribute to TGFβ-induced nuclear deformation

In addition to alterations in the property of the nuclear lamina, emerging evidence suggests that actomyosin-mediated contractility and content of heterochromatin and euchromatin may be involved in nuclear deformation.[76–78] Because EMT is characterized by both increased F-actin and chromatin-reconfigurations,[4,68,79,80] the possibilities of these two events to be involved in the TGFβ-induced nuclear deformation were examined. We found that TGFβ-induced nuclear deformation was partially reduced by the F-actin depolymerization agent cytochalasin D (Figure S4A) and the inhibitors that suppressed actomyosin-mediated contractility,[81] including the ROCK inhibitor Y27632, the MLCK inhibitor ML-7, and the myosin II inhibitor blebbistatin (Figure S4B). These results indicated that the mechanical force generated by actomyosin-mediated contractility contributes to TGFβ-induced nuclear deformation.

Next, the content of heterochromatin was examined by immunofluorescence staining with an antibody specific to the tri-methylation of lysine 27 on histone H3 protein (H3K27me3), a main heterochromatin marker. We found that the intensity of H3K27me3 was 1.45-fold increased on TGFβ treatment (Figures 5A and 5B), which was preferentially accumulated in the protruded region rather than the concave region of deformed nuclei (Figures 5A and 5C). Furthermore, to determine whether the increased level of heterochromatin is involved in nuclear deformation, chromatin was de-compacted by 3-Deazaneplanocin-A (DZNep), a methyltransferase inhibitor that decreases heterochromatin.[77] We found that DZNep suppressed the increase of H3K27me3 and partially suppressed nuclear deformation on TGFβ treatment (Figure 5D). In contrast, methylstat, a histone demethylase inhibitor,[77] was able of increase H3K27me3 and cause nuclear deformation in the absence of TGFβ treatment (Figure 5E). Together, these results suggest that the increased heterochromatin may contribute to nuclear deformation during TGFβ-induced EMT.

Nuclear deformation is associated with genome instability during EMT

The biological significance of nuclear deformation in TGFβ-induced EMT was examined. TGFβ prominently induced mesenchymal cell markers fibronectin and F-actin in A549 cells, no matter whether their nuclei were deformed (Figure S5). Although the lamin A S390A mutant protected A549 cells against nuclear deformation on TGFβ stimulation, as described in Figures 2C, S6A and S6B, it failed to prevent the disruption of cell-cell junctions on TGFβ stimulation (Figures S6C and S6D). In addition, the S390A mutant did not affect TGFβ-promoted cell migration through a 5-μm porous membrane (Figure S6E). These results together

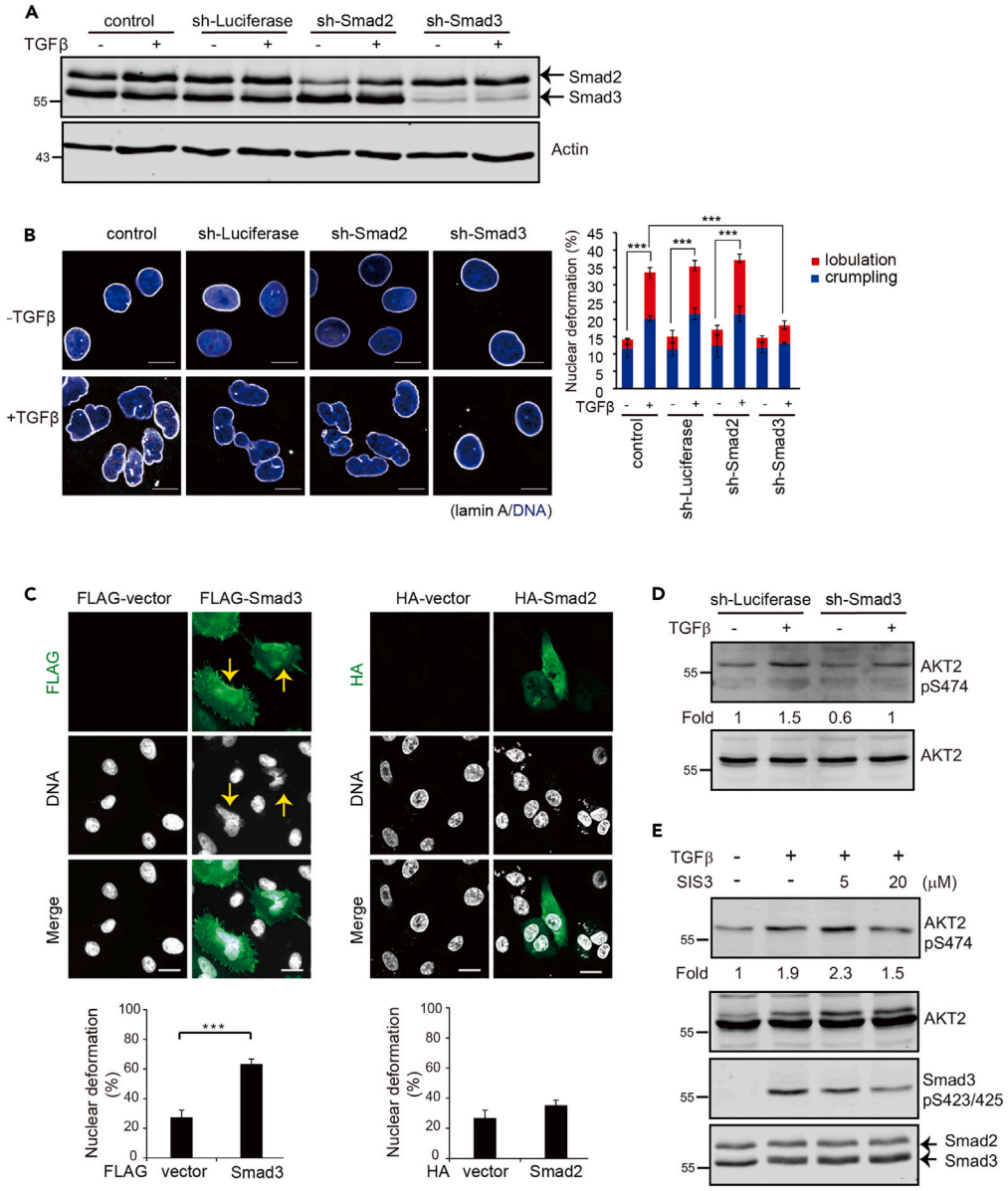

Figure 4. Smad3 contributes to AKT2 phosphorylation and TGFβ-induced nuclear deformation

(A) A549 cells were infected with lentiviruses encoding shRNAs specific to luciferase (sh-Luciferase), Smad2 (sh-Smad2), or Smad3 (sh-Smad3). The cells were treated with (+) or without (–) TGFβ for 24 h and lysed. An equal amount of whole cell lysates was analyzed by immunoblotting with anti-Smad2/3 or anti-actin antibody.

(B) The cells as described in (A) were treated with or without TGFβ for 24 h and stained for lamin A (white) and DNA (blue). Scale bars, 10 μm. The percentage of the cells with a crumpled or lobulated nucleus was measured ($n \geq 600$).

(C) A549 cells were transiently transfected with the plasmid encoding FLAG-Smad3 or HA-Smad2 for 24 h, and then stained for FLAG (green), HA (green), and DNA (white). Scale bars, 20 μm. The percentage of the transfection-positive cells with a deformed nucleus was measured ($n \geq 269$).

(D) A549 cells expressing shRNAs to luciferase or Smad3 were treated with or without TGFβ for 1 h. An equal amount of whole cell lysates was analyzed by immunoblotting with anti-AKT2 pS474 or anti-AKT2 antibody. The phosphorylation of AKT2 at Ser474 was quantified and expressed as –fold relative to the level of the control.

(E) A549 cells were pre-treated with the Smad3 inhibitor SIS3 for 4 h and then co-treated with TGFβ for 1 h. An equal amount of whole cell lysates was analyzed by immunoblotting with the antibodies as indicated. The phosphorylation of AKT2 at Ser474 was quantified and expressed as –fold relative to the level of the control. Data information: In B and C, values (means ± SD) were from three independent experiments. ***$p < 0.001$. See also Figure S3.

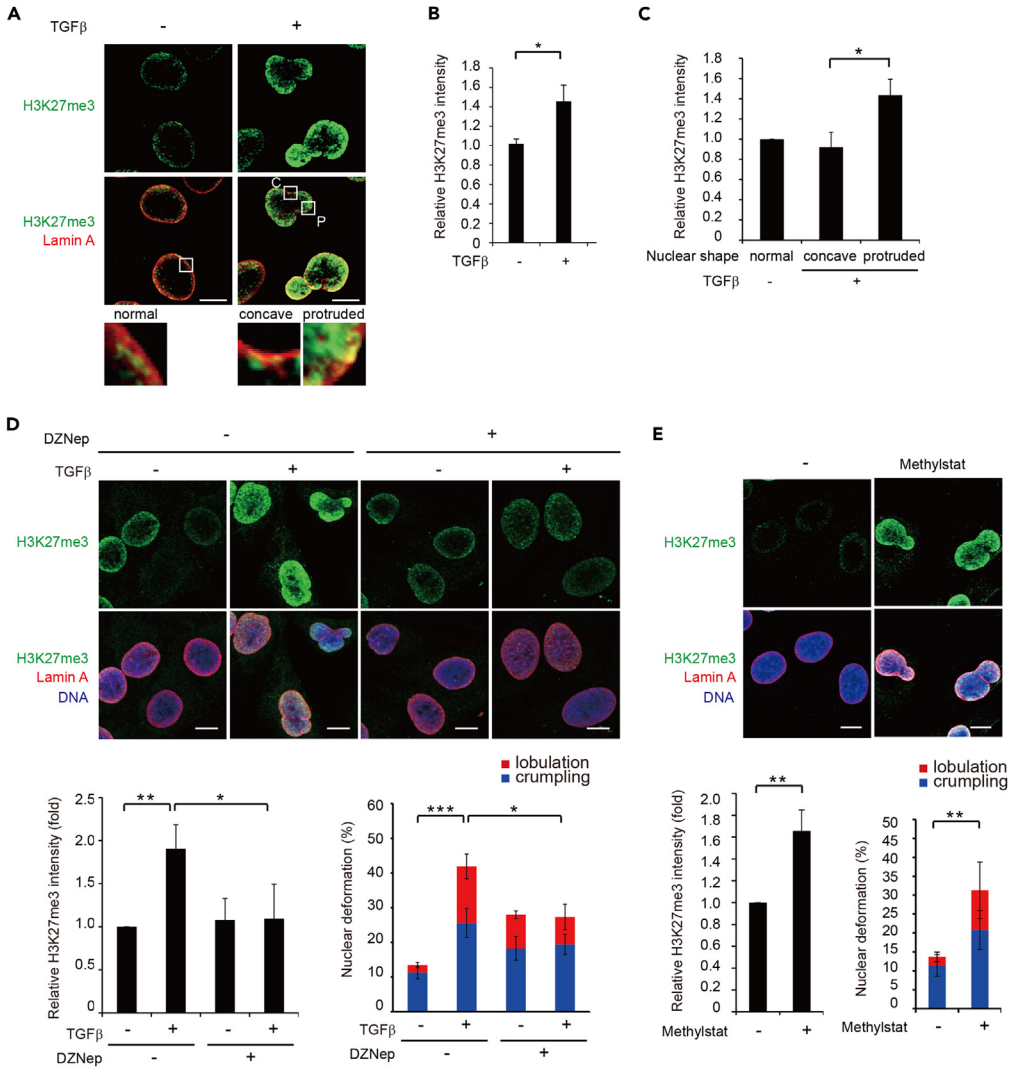

Figure 5. Increased heterochromatin formation contributes to TGFβ-induced nuclear deformation

(A) A549 cells were treated with TGFβ for 48 h and stained for H3K27me3 (green) and lamin A (red). The insets are enlarged to show heterochromatins beneath a normal nuclear region, or the concave (labeled as C) or protruded (labeled as P) region of a deformed nucleus. Scale bars, 10 μm.

(B) The relative nuclear intensity of H3K27me3 was measured according to the immunofluorescence images from panel A (n = 120 cells).

(C) The H3K27me3 intensity of the normal, concave or protruded region (4.694 μm^2) of the nucleus was measured from the immunofluorescence images in panel A (n ≥ 67 cells).

(D) A549 cells were pre-treated with DZNep (10 μM) for 0.5 h and co-treated with TGFβ for 48 h. The cells were stained for H3K27me3 (green), lamin A (red), and DAPI (blue). Scale bars, 10 μm. The graphs show the nuclear H3K27me3 intensity (n ≥ 125 cells) and the nuclear deformation rate (n ≥ 376 cells), respectively.

(E) A549 cells were treated with methylstat (10 μM) for 24 h and stained for H3K27me3 (green), lamin A (red), and DAPI (blue). Scale bars, 10 μm. The graphs show the nuclear H3K27me3 intensity (n ≥ 118 cells) and the nuclear deformation rate (n ≥ 354 cells), respectively. Data information: In B, C, D and E, values (means ± SD) were from three independent experiments. *p < 0.05, **p < 0.01, ***p < 0.001. See also Figure S4.

indicate that nuclear deformation is not associated with certain EMT phenotypes, including fibronectin expression, loss of cell-cell junctions, and increased cell migration.

Genome instability is one of characteristics during TGFβ-induced EMT.[2,82,83] In this study, we found that TGFβ induced micronuclei in A549 cells, which was abolished by the AKT inhibitor MK2206 (Figure 6A).

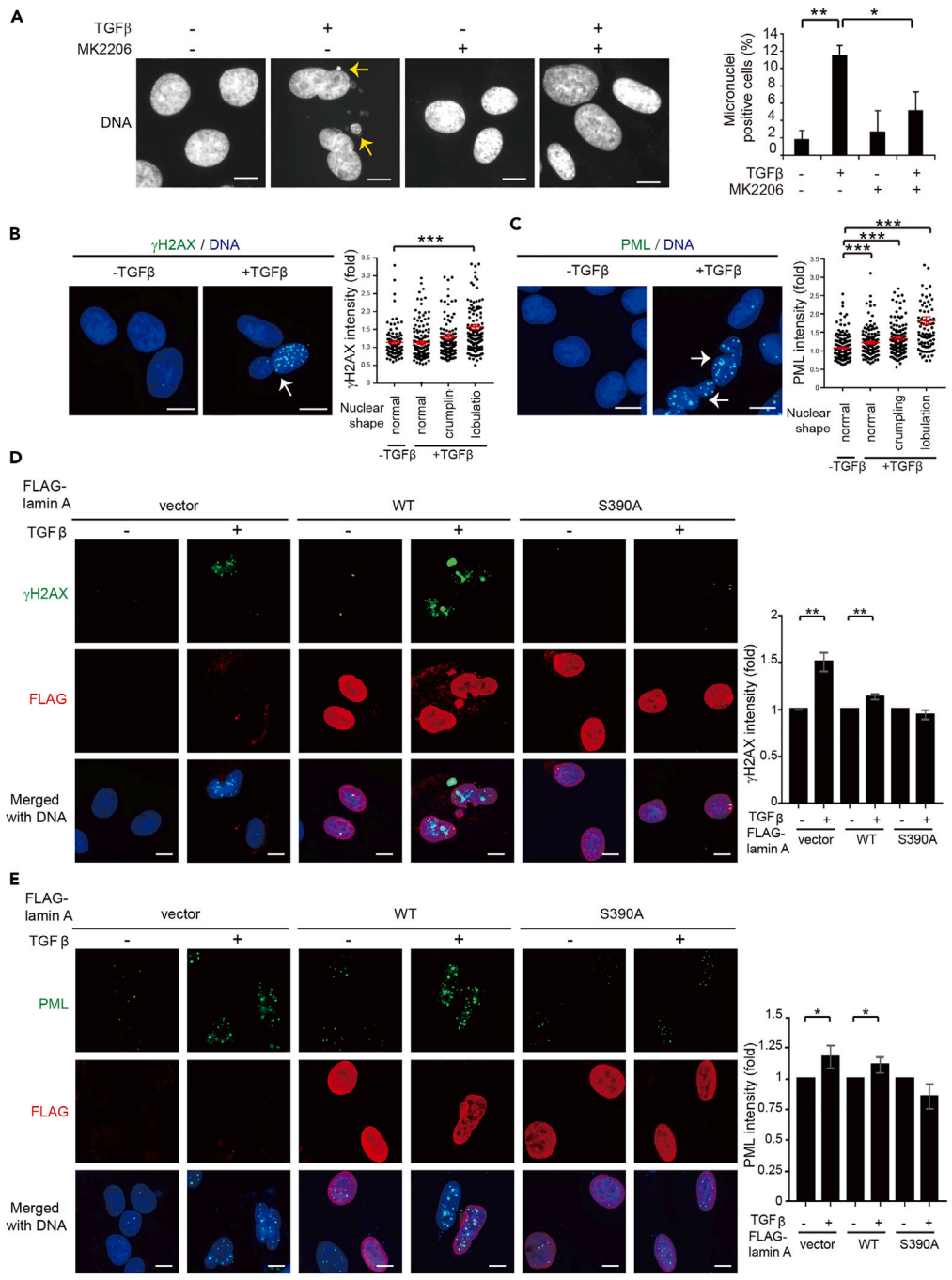

Figure 6. TGFβ-induced nuclear deformation is tightly associated with genome instability

(A) A549 cells were pre-treated with MK2206 for 1 h, co-treated with TGFβ for 72 h, and stained for DNA. The arrows indicate micronuclei. Scale bars, 10 μm. The percentage of the cells with a micronucleus was measured ($n \geq 315$).

(B) A549 cells were treated with or without TGFβ for 72 h and stained for γH2AX and DNA. The arrow indicates a deformed nucleus with γH2AX. Scale bars, 10 μm. The fluorescence intensity of γH2AX in the normal, crumpled, and lobulated nucleus was measured ($n \geq 139$) and expressed as –fold relative to the average of the control.

(C) A549 cells were treated with or without TGFβ for 72 h and stained for PML and DNA. The arrows indicate deformed nuclei with PML. Scale bars, 10 μm. The fluorescence intensity of PML in the normal, crumpled, and lobulated nucleus was measured ($n \geq 97$) and expressed as –fold relative to the average of the control.

(D) FLAG-lamin A or the S390A mutant was transiently expressed in A549 cells for 24 h and then treated with TGFβ for 48 h. The cells were stained for γH2AX (green), FLAG-lamin A (red), and DNA (blue). Representative images are shown. Scale

Figure 6. *Continued*

bars, 10 μm. The fluorescence intensity of γH2AX in the transfection-positive cells was measured (n ≥ 210) and expressed as –fold relative to the control group.

(E) The cells as described in (D) were stained for PML (green), FLAG-lamin A (red), and DNA (blue). Representative images are shown. Scale bars, 10 μm. The fluorescence intensity of PML in the transfection-positive cells was measured (n ≥ 130) and expressed as –fold relative to the control group. Data information: In A, D and E values (means ± SD) were from three independent experiments. In B and C, values (means ± SEM) were from three independent experiments. *p < 0.05, **p < 0.01, ***p < 0.001. See also Figures S5–S7.

In addition, the deformed nuclei by TGFβ were found to harbor more DNA damage (Figures 6B and 6C), as revealed by nuclear accumulation of two DNA-lesion markers γH2AX and PML.[84,85] These results render it possible that nuclear deformation may be linked to genome instability during EMT. Indeed, the S390A mutant, which protected A549 cells against TGFβ-induced nuclear deformation, inhibited the induction of γH2AX and PML on TGFβ stimulation (Figures 6D and 6E). Likewise, inhibition of nuclear deformation by the AKT inhibitor MK2206 suppressed TGFβ-induced γH2AX and PML (Figures S7A and S7B). Moreover, overexpression of HA-AKT2, but not HA-AKT1, was sufficient to induce nuclear deformation and increased γH2AX in A549 cells without TGFβ treatment (Figure S7C). These results together indicate that AKT2-mediated nuclear deformation is tightly associated with genome instability during TGFβ-induced EMT.

Nuclear deformation causes defective DNA repair mechanisms, leading to genome instability

TGFβ-induced genome instability can be attributed to defective DNA repair mechanisms.[82,83,86] As described previously,[87] a fraction of ATR, a DNA repair protein, was found to localize at the nuclear lamina of the nucleus with normal shape (Figure S8). However, ATR was no longer localized at the nuclear lamina of the deformed nucleus on TGFβ stimulation, which was restored by the AKT inhibitor MK2206 (Figure 7A) and the lamin A S390A mutant (Figure 7B). The DNA damage caused by hydroxyurea (HU) is known to trigger ATR-mediated DNA repair.[88] We found that the loss of ATR at the nuclear lamina by TGFβ abrogated the repair for the DNA damage elicited by HU, as revealed by nuclear accumulation of γH2AX (Figure S9A). Moreover, we found that the level of the DNA repair protein 53BP1 was decreased in the deformed nuclei on TGFβ stimulation (Figure 7C), which was restored by the AKT inhibitor MK2206 (Figure 7C) and the lamin A S390A mutant (Figure 7D). The DNA damage caused by etoposide is known to trigger 53BP1-mediated DNA repair.[89,90] We found that the decreased level of 53BP1 caused by TGFβ hampered the repair for the DNA damage elicited by etoposide, as revealed by nuclear accumulation of γH2AX (Figure S9B). These results suggest that nuclear deformation may cause mis-localization and/or degradation of certain DNA repair proteins, such as ATR and 53BP1, and thereby abrogate the DNA repair mechanism, leading to a loss of genome integrity.

DISCUSSION

Nuclear deformation or dysmorphia has long been considered to associate with the malignancy of tumors. However, its underlying mechanism and biological significance in tumorigenesis remain unclear. In the present study, we show that nuclear deformation, concomitant with defective nuclear lamina, is one of the characteristics during TGFβ-induced EMT. It is tightly associated with genome instability, but not other EMT phenotypes, including loss of cell-cell junctions, mesenchymal morphological changes, increased fibronection expression, and elevated cell migration. As depicted in Figure 8, on TGFβ stimulation, AKT2 is activated in a PI3K- and Smad3-dependent manner, which then translocates into the nucleus where it directly phosphorylates lamin A mainly at Ser390. The increased phosphorylation of lamin A at Ser390 may result in relaxed nuclear lamina. Subsequently, the TGFβ-induced increases in actomyosin-mediated contractility and heterochromatin may respectively exert inward and outward force to cause nuclear deformation, accompanied by defects in the nuclear lamina. The defects in the nuclear lamina then induce mis-localization and/or downregulation of DNA repair proteins, such as ATR and 53BP1, finally leading to genome instability.

Our results reveal that AKT2-mediated phosphorylation of lamin A at Ser390 is correlated with increased solubility of lamin A and its re-distribution from the lamina to nucleoplasm on TGFβ stimulation. This is not surprising because the serine phosphorylation of lamin A at Ser22, 390, 392, or 404 is known to have an adverse effect on lamin A assembly.[43,46] However, to our surprise, expression of the lamin A S390A mutant alone is sufficient to protect the cells against nuclear deformation induced by TGFβ (Figure 2E). This strongly supports that AKT2-mediated phosphorylation of lamin A at Ser390 is a prerequisite for TGFβ to induce nuclear deformation. Nevertheless, it is generally believed that besides defects in the nuclear lamina organization, other mechanical forces that directly apply on the nucleus are needed to cause nuclear deformation. In other words, phosphorylation of lamin A by itself is not sufficient to cause nuclear deformation. The forces that affect nuclear morphology can

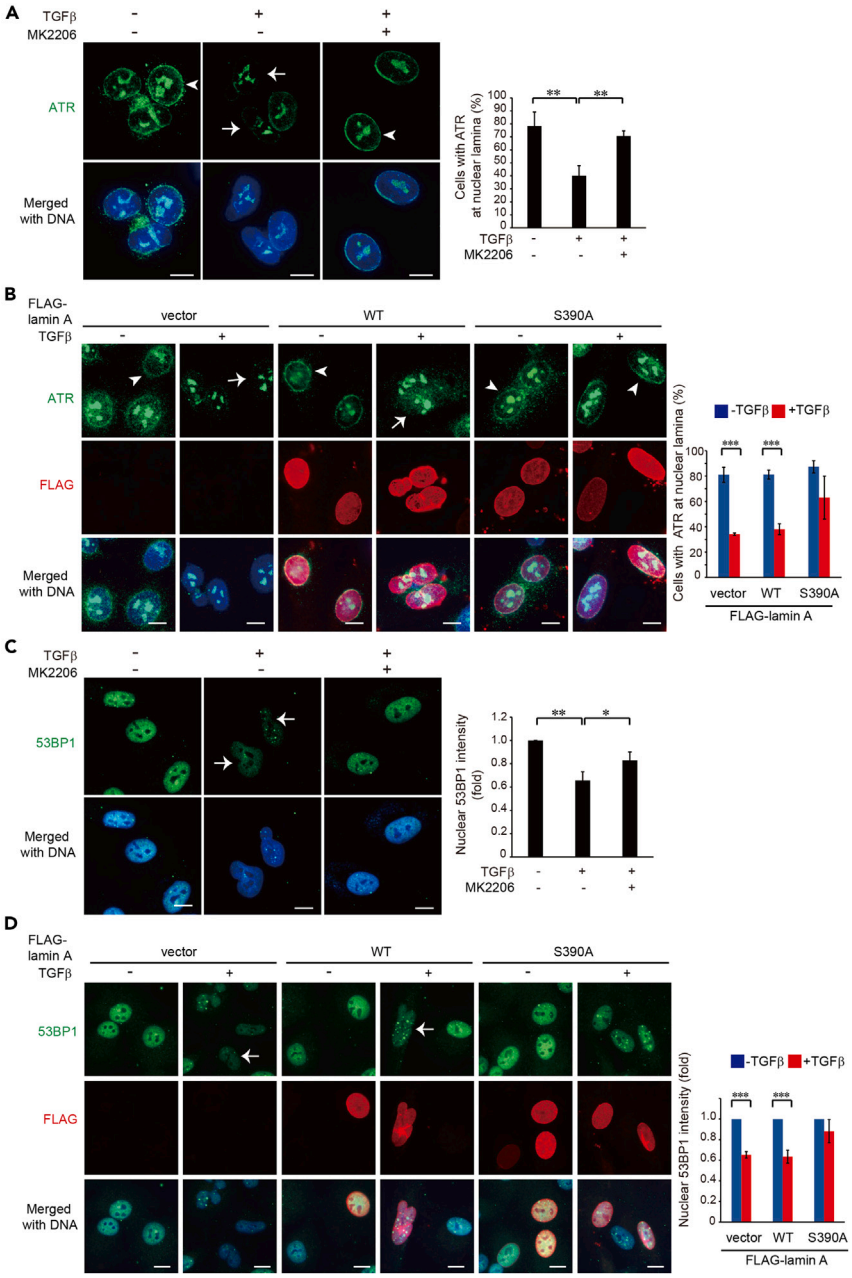

Figure 7. Nuclear deformation causes a mis-localization of ATR and decreased expression of 53BP1

(A) A549 cells were treated with (+) or without (–) TGFβ and the AKT inhibitor MK2206 (5 μM) for 72 h and stained for ATR and DNA. The arrowheads indicate the nucleus with a fraction of ATR localized at the nuclear lamina. The arrows indicate the deformed nucleus without ATR at the nuclear lamina. Scale bars, 10 μm. The percentage of the cells with ATR at the nuclear lamina was measured ($n \geq 236$).

(B) FLAG-lamin A or the S390A mutant was transiently expressed in A549 cells for 24 h and then treated with or without TGFβ for 48 h. The cells were stained for ATR (green), FLAG-lamin A (red), and DNA (blue). The arrowheads indicate the nucleus with a fraction of ATR localized at the nuclear lamina. The arrows indicate the deformed nucleus without ATR at the nuclear lamina. Scale bars, 10 μm. The percentage of the transfected cells with ATR at the nuclear lamina was measured ($n \geq 88$).

(C) The cells as described in (A) were stained for 53BP1 and DNA. The arrows indicate the deformed nucleus with a lower fluorescence intensity of 53BP1. Scale bars, 10 μm. The fluorescence intensity of 53BP1 in the nucleus was measured ($n \geq 145$) and expressed as –fold relative to the control.

Figure 7. *Continued*

(D) The cells as described in (C) were stained for 53BP1 (green), FLAG-lamin A (red), and DNA (blue). The arrows indicate the deformed nucleus with a lower fluorescence intensity of 53BP1. Scale bars, 10 μm. The fluorescence intensity of 53BP1 in the nucleus was measured (n ≥ 86) and expressed as –fold relative to the control group. Data information: In A to D, values (means ± SD) were from three independent experiments. *p < 0.05, **p < 0.01, ***p < 0.001. See also Figures S8 and S9.

arise from both outside and inside the nucleus. Outside the nucleus, actin-based nucleus confinement was reported to induce nuclear envelope rupture in human osteosarcoma U2OS cells.[91] In addition, the unrestrained actomyosin contractility caused by loss of myosin phosphatases was found to drive cancer cells nuclear deformation, nuclear envelop rupture, and genome instability.[78] Inside the nucleus, chromatin histone modification state or compositional changes in the chromatin may affect nuclear rigidity. It was reported that chromatin compaction via increased heterochromatin confers rigidity to the nucleus.[77] A recent study reported that compositional changes in the chromatin by upregulated expression of histone H3.3, a histone H3 variant,[92] contribute to TGFβ-induced nuclear deformation in liver cancer Huh7 cells.[68]

In the present study, we demonstrated that actomyosin contractility and increased heterochromatin content contribute to nuclear deformation during TGFβ-induced EMT (Figures 5 and S4). However, the underlying mechanisms of how these two events affect nuclear morphology in context with alterations in the nuclear lamina during TGFβ-induced EMT remain unclear. Heterochromatin is scattered throughout the nucleus or accumulated adjacent to the nuclear envelope, where it is tethered by lamin A and its associated proteins.[93,94] It was shown that decreased tethering of heterochromatin at the nuclear envelope leads to a softer and deformable nucleus.[95] In this study, we observed that heterochromatin is apparently accumulated at the protruded region of the deformed nucleus on TGFβ stimulation (Figure 5C). It is possible that lamin A phosphorylation at S390 may affect the tethering of heterochromatin with the nuclear lamina, which could cause an uneven rigidity on the nucleus and finally lead to nuclear deformation. Intriguingly, it was reported that the nuclear deformation caused by F-actin is associated with heterochromatin formation during confined cell migration.[96,97] It remains unknown whether actin-based nucleus confinement could affect the tethering of heterochromatin with the nuclear lamina and the rigidity of the nuclear envelope.

The present study reveals that Smad3, but not Smad2, is required for the activation of AKT2 on TGFβ stimulation (Figure 4). This is in accordance with previous findings that AKT interacts with Smad3, but not Smad2, on TGFβ stimulation,[98] and inhibition of Smad3 suppresses AKT phosphorylation induced by TGFβ.[99] However, the molecular mechanism of how Smad3 facilitates AKT2 activation on TGFβ stimulation remains unclear. Because the Smad3-specfic inhibitor SIS3 that inhibits Smad3 phosphorylation at Ser423/425 suppressed the AKT2 activation on TGFβ stimulation (Figure 4E), it is possible that phosphorylation of Smad3 may be necessary for it to interact with and activate AKT2. As depicted in Figure 8, phosphorylated Smad3 may recruit AKT2 to the TGFβ receptor, by which AKT2 is in close proximity to its upstream activator PI3K and the PI3K lipid products (e.g., phosphatidylinositol 3,4,5-trisphosphate, PIP3), which are known to bind to the PH domain of AKT for its activation on the plasma membrane.[27] Of note, the phosphorylation and nuclear translocation of Smad3 were not affected by AKT inhibition (Figure S3). It will be of interest to examine whether activated AKT2 separates from Smad3 and then translocates into the nucleus by itself, or AKT2 retains in a complex form with Smad3 during nuclear translocation. Intriguingly, R-Smads were reported to be sequestered by the nuclear lamina.[100] How the transcriptional activities of R-Smads are regulated in context with AKT2-mediated lamin A phosphorylation and nuclear deformation during TGFβ-induced EMT remains to be explored.

We demonstrate in this study that both AKT1 and AKT2 are activated on TGFβ stimulation, but only AKT2 is responsible for increased lamin A phosphorylation at Ser390 (Figure 3). The *in vitro* kinase assay clearly showed that AKT2, but not AKT1, directly phosphorylated lamin A at Ser390, whereas both AKT isozymes phosphorylated lamin A at Ser404 to similar extent (Figure 3H). A possible explanation for this is that lamin A Ser390 (RLRLS^{390}) may be at an atypical phosphorylation motif (R-x-R-x-S*, where x represents any amino acid and the asterisk indicates the site of phosphorylation) specific for AKT2, whereas Ser404 (RGRASS^{404}) is at an AKT consensus phosphorylation motif (R-x-R-x-x-S*/T*). In addition to Ser390 and Ser404, Ser22 (S^{22}PTR) and Ser392 (S^{392}PTS) are prominent phosphorylation sites of lamin A, both of which are at a CDK consensus sequence (S/T*-P, or S/T*-P-x-K/R). This can explain why both AKT1 and AKT2 failed to phosphorylate lamin A at Ser22 in our *in vitro* kinase assay (Figure 3H). Previous studies indicate that AKT isoforms perform distinct functions,[30,34,35] partly because of their different substrate specificity.[101–103] AKT2 has been shown to promote tumor malignancy.[33–35] It is not known whether the phosphorylation of lamin A Ser390 by AKT2 is generally associated with the role of AKT2 in this regard.

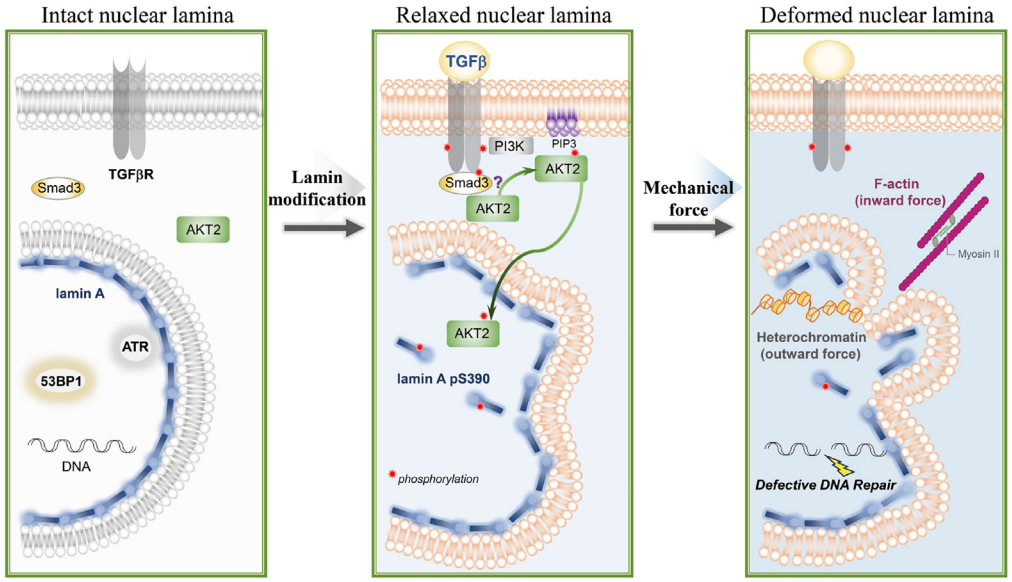

Figure 8. Illustration of how TGFβ induces nuclear deformation and its link to genome instability

The intact nuclear lamina is important for proper localization and expression of certain DNA repair proteins, such as ATR and 53BP1 (left panel). On TGFβ stimulation, Smad3 is phosphorylated and facilitates AKT2 activation by an unknown mechanism. It is possible that phosphorylated Smad3 may recruit AKT2 to the TGFβ receptor in a close proximity to its upstream activator PI3K and the PI3K lipid products (*e.g.* phosphatidylinositol 3,4,5-trisphosphate, PIP3). The activated AKT2 translocates into the nucleus where it directly phosphorylates lamin A mainly at Ser390. The increased phosphorylation of lamin A at Ser390 causes the relaxation of the nuclear lamina (middle panel). Meanwhile, the contractile F-actin and compact heterochromatin provide mechanical forces to cause nuclear deformation and defects in the nuclear lamina. The defects in the nuclear lamina then induce mis-localization and/or downregulation of ATR and 53BP1, finally leading to genome instability (right panel).

Besides observed in some cancer cells, nuclear deformation is the hallmark of the cells derived from patients with laminopathies, a group of rare genetic disorders caused by mutations in genes encoding lamins.[52] Increasing evidence indicates that the nuclear lamina serves as a subcellular compartment important for the choice of DNA repair pathway and maintenance of genome integrity.[59,63,104] For instance, lamin A deficiency results in mis-localization or degradation of nuclear ATR[61,62] and 53BP1.[58,105] Likewise, we found in this study that TGFβ caused mis-localization of ATR and a decreased level of 53BP1, both of which were restored by the lamin A S390A mutant that provided resistance to nuclear deformation on TGFβ stimulation (Figure 7). Our results thus suggest that the defects in the nuclear lamina caused by mutations in lamin genes (e.g., laminopathies) or post-translational modifications of lamins on extracellular cues (e.g., TGFβ stimulation) may impair ATR- and 53BP1-mediated DNA repair, leading to genome instability. Because TGFβ has been shown to downregulate the expression and/or activity of several other DNA repair proteins, such as ATM, BRCA1, and Rad51,[82,83,86] it should be aware that the loss of the genome integrity during TGFβ-induced EMT may not be completely attributed to the defects in the nuclear lamina. In summary, the present study not only unravels a significant role of AKT2 in lamin A phosphorylation and nuclear deformation, but also demonstrates a tight association of nuclear deformation with genome instability during TGFβ-induced EMT.

Limitations of the study

Our results shown in this study were derived from cultured cancer cell lines. Therefore, the molecular mechanism and clinical significance proposed by this study await further *in vivo* studies for validations.

STAR★METHODS

Detailed methods are provided in the online version of this paper and include the following:

- KEY RESOURCES TABLE
- RESOURCE AVAILABILITY
  - Lead contact
  - Materials availability

SUPPLEMENTAL INFORMATION

Supplemental information can be found online at https://doi.org/10.1016/j.isci.2023.106992.

ACKNOWLEDGMENTS

This work was supported by the National Science and Technology Council, Taiwan (grant number 108-2320-B-010-015-MY3) and the Cancer Progression Research Center (111W31101) and the Cancer and Immunology Research Center (112W31101), National Yang Ming Chiao Tung University from the Featured Areas Research Center Program within the framework of the Higher Education Sprout Project by the Ministry of Education in Taiwan.

AUTHOR CONTRIBUTIONS

J-R.F.: Data curation, formal analysis, investigation, and writing—original draft.

S-N.C.: Investigation.

C-T.C.: Investigation.

H-C.C.: Conceptualization, supervision, funding acquisition, project administration, and writing–review and editing.

DECLARATION OF INTERESTS

The authors declare no competing interests.

INCLUSION AND DIVERSITY

We support inclusive, diverse, and equitable conduct of research.

Received: February 3, 2023
Revised: May 4, 2023
Accepted: May 25, 2023
Published: May 29, 2023

REFERENCES

1. Nieto, M.A., Huang, R.Y.-J., Jackson, R.A., and Thiery, J.P. (2016). EMT: 2016. Cell *166*, 21–45. https://doi.org/10.1016/j.cell.2016.06.028.

2. Comaills, V., Kabeche, L., Morris, R., Buisson, R., Yu, M., Madden, M.W., LiCausi, J.A., Boukhali, M., Tajima, K., Pan, S., et al. (2016). Genomic instability is induced by persistent proliferation of cells undergoing epithelial-to-mesenchymal transition. Cell Rep. *17*, 2632–2647. https://doi.org/10.1016/j.celrep.2016.11.022.

3. Grünert, S., Jechlinger, M., and Beug, H. (2003). Diverse cellular and molecular mechanisms contribute to epithelial plasticity and metastasis. Nat. Rev. Mol. Cell Biol. *4*, 657–665. https://doi.org/10.1038/nrm1175.

4. Lamouille, S., Xu, J., and Derynck, R. (2014). Molecular mechanisms of epithelial–mesenchymal transition. Nat. Rev. Mol. Cell Biol. *15*, 178–196. https://doi.org/10.1038/nrm3758.

5. Sieber, O.M., Heinimann, K., and Tomlinson, I.P.M. (2003). Genomic instability—the engine of tumorigenesis? Nat. Rev. Cancer *3*, 701–708. https://doi.org/10.1038/nrc1170.

6. Dey, P. (2010). Cancer nucleus: morphology and beyond. Diagn. Cytopathol. *38*, 382–390. https://doi.org/10.1002/dc.21234.

7. True, L.D., and Jordan, C.D. (2008). The cancer nuclear microenvironment: interface between light microscopic cytology and molecular phenotype. J. Cell. Biochem. *104*, 1994–2003. https://doi.org/10.1002/jcb.21478.

8. Zink, D., Fischer, A.H., and Nickerson, J.A. (2004). Nuclear structure in cancer cells. Nat. Rev. Cancer *4*, 677–687. https://doi.org/10.1038/nrc1430.

9. Tam, S.Y., Wu, V.W.C., and Law, H.K.W. (2020). Hypoxia-induced epithelial-mesenchymal transition in cancers: HIF-1α and beyond. Front. Oncol. *10*, 486–496. https://doi.org/10.3389/fonc.2020.00486.

10. Piek, E., Moustakas, A., Kurisaki, A., Heldin, C.-H., and ten Dijke, P. (1999). TGF-(beta) type I receptor/ALK-5 and Smad proteins mediate epithelial to mesenchymal transdifferentiation in NMuMG breast epithelial cells. J. Cell Sci. *112*, 4557–4568. https://doi.org/10.1242/jcs.112.24.4557.

11. Valcourt, U., Kowanetz, M., Niimi, H., Heldin, C.-H., and Moustakas, A. (2005). TGF-β and the Smad signaling pathway support transcriptomic reprogramming during epithelial-mesenchymal cell transition. Mol. Biol. Cell *16*, 1987–2002. https://doi.org/10.1091/mbc.e04-08-0658.

12. Derynck, R., and Zhang, Y.E. (2003). Smad-dependent and Smad-independent pathways in TGF-β family signalling. Nature *425*, 577–584. https://doi.org/10.1038/nature02006.

13. Vincent, T., Neve, E.P.A., Johnson, J.R., Kukalev, A., Rojo, F., Albanell, J., Pietras, K., Virtanen, I., Philipson, L., Leopold, P.L., et al. (2009). A SNAIL1–SMAD3/4 transcriptional repressor complex promotes TGF-β mediated epithelial–mesenchymal transition. Nat. Cell Biol. *11*, 943–950. https://doi.org/10.1038/ncb1905.

14. Brown, K.A., Pietenpol, J.A., and Moses, H.L. (2007). A tale of two proteins: differential roles and regulation of Smad2 and Smad3 in TGF-β signaling. J. Cell. Biochem. *101*, 9–33. https://doi.org/10.1002/jcb.21255.

15. Petersen, M., Pardali, E., van der Horst, G., Cheung, H., Van Den Hoogen, C., Van Der Pluijm, G., and Ten Dijke, P. (2010). Smad2 and Smad3 have opposing roles in breast cancer bone metastasis by differentially affecting tumor angiogenesis. Oncogene *29*, 1351–1361. https://doi.org/10.1038/onc.2009.426.

16. Piek, E., Ju, W.J., Heyer, J., Escalante-Alcalde, D., Stewart, C.L., Weinstein, M., Deng, C., Kucherlapati, R., Böttinger, E.P., and Roberts, A.B. (2001). Functional characterization of transforming growth factor β signaling in Smad2-and Smad3-deficient fibroblasts. J. Biol. Chem. *276*, 19945–19953. https://doi.org/10.1074/jbc.M102382200.

17. Zhang, Y.E. (2017). Non-Smad signaling pathways of the TGF-β family. Cold Spring Harbor Perspect. Biol. *9*, a022129–a022148. https://doi.org/10.1101/cshperspect.a022129.

18. Atfi, A., Djelloul, S., Chastre, E., Davis, R., and Gespach, C. (1997). Evidence for a role of Rho-like GTPases and stress-activated protein kinase/c-Jun N-terminal kinase (SAPK/JNK) in transforming growth factor β-mediated signaling. J. Biol. Chem. *272*, 1429–1432. https://doi.org/10.1074/jbc.272.3.1429.

19. Hanafusa, H., Ninomiya-Tsuji, J., Masuyama, N., Nishita, M., Fujisawa, J., Shibuya, H., Matsumoto, K., and Nishida, E. (1999). Involvement of the p38 mitogen-activated protein kinase pathway in transforming growth factor-β-induced gene expression. J. Biol. Chem. *274*, 27161–27167. https://doi.org/10.1074/jbc.274.38.27161.

20. Hartsough, M.T., and Mulder, K.M. (1995). Transforming growth factor β activation of p44mapk in proliferating cultures of epithelial cells. J. Biol. Chem. *270*, 7117–7124. https://doi.org/10.1074/jbc.270.13.7117.

21. Zavadil, J., Bitzer, M., Liang, D., Yang, Y.-C., Massimi, A., Kneitz, S., Piek, E., and Böttinger, E.P. (2001). Genetic programs of epithelial cell plasticity directed by transforming growth factor-β. Proc. Natl. Acad. Sci. USA *98*, 6686–6691. https://doi.org/10.1073/pnas.111614398.

22. Bakin, A.V., Tomlinson, A.K., Bhowmick, N.A., Moses, H.L., and Arteaga, C.L. (2000). Phosphatidylinositol 3-kinase function is required for transforming growth factor β-mediated epithelial to mesenchymal transition and cell migration. J. Biol. Chem. *275*, 36803–36810. https://doi.org/10.1074/jbc.M005912200.

23. Lamouille, S., Connolly, E., Smyth, J.W., Akhurst, R.J., and Derynck, R. (2012). TGF-β-induced activation of mTOR complex 2 drives epithelial–mesenchymal transition and cell invasion. J. Cell Sci. *125*, 1259–1273. https://doi.org/10.1242/jcs.095299.

24. Lamouille, S., and Derynck, R. (2007). Cell size and invasion in TGF-β–induced epithelial to mesenchymal transition is regulated by activation of the mTOR pathway. J. Cell Biol. *178*, 437–451. https://doi.org/10.1083/jcb.200611146.

25. Singha, P.K., Pandeswara, S., Geng, H., Lan, R., Venkatachalam, M.A., and Saikumar, P. (2014). TGF-β induced TMEPAI/PMEPA1 inhibits canonical Smad signaling through R-Smad sequestration and promotes non-canonical PI3K/Akt signaling by reducing PTEN in triple negative breast cancer. Genes Cancer *5*, 320–336. https://doi.org/10.18632/genesandcancer.30.

26. Vo, B.T., Morton, D., Jr., Komaragiri, S., Millena, A.C., Leath, C., and Khan, S.A. (2013). TGF-β effects on prostate cancer cell migration and invasion are mediated by PGE2 through activation of PI3K/AKT/mTOR pathway. Endocrinology *154*, 1768–1779. https://doi.org/10.1210/en.2012-2074.

27. Manning, B.D., and Toker, A. (2017). AKT/PKB signaling: navigating the network. Cell *169*, 381–405. https://doi.org/10.1016/j.cell.2017.04.001.

28. Brodbeck, D., Cron, P., and Hemmings, B.A. (1999). A human protein kinase Bγ with regulatory phosphorylation sites in the activation loop and in the C-terminal hydrophobic domain. J. Biol. Chem. *274*, 9133–9136. https://doi.org/10.1074/jbc.274.14.9133.

29. Yang, Z.-Z., Tschopp, O., Hemmings-Mieszczak, M., Feng, J., Brodbeck, D., Perentes, E., and Hemmings, B.A. (2003). Protein kinase Bα/Akt1 regulates placental development and fetal growth. J. Biol. Chem. *278*, 32124–32131. https://doi.org/10.1074/jbc.M302847200.

30. Toker, A., and Marmiroli, S. (2014). Signaling specificity in the Akt pathway in biology and disease. Adv. Biol. Regul. *55*, 28–38. https://doi.org/10.1016/j.jbior.2014.04.001.

31. Chen, W.S., Xu, P.-Z., Gottlob, K., Chen, M.-L., Sokol, K., Shiyanova, T., Roninson, I., Weng, W., Suzuki, R., Tobe, K., et al. (2001). Growth retardation and increased apoptosis in mice with homozygous disruption of the Akt1 gene. Genes Dev. *15*, 2203–2208. https://doi.org/10.1101/gad.913901.

32. Cho, H., Thorvaldsen, J.L., Chu, Q., Feng, F., and Birnbaum, M.J. (2001). Akt1/PKBα is required for normal growth but dispensable for maintenance of glucose homeostasis in mice. J. Biol. Chem. *276*, 38349–38352. https://doi.org/10.1074/jbc.C100462200.

33. Irie, H.Y., Pearline, R.V., Grueneberg, D., Hsia, M., Ravichandran, P., Kothari, N., Natesan, S., and Brugge, J.S. (2005). Distinct roles of Akt1 and Akt2 in regulating cell migration and epithelial–mesenchymal transition. J. Cell Biol. *171*, 1023–1034. https://doi.org/10.1083/jcb.200505087.

34. Riggio, M., Perrone, M.C., Polo, M.L., Rodriguez, M.J., May, M., Abba, M., Lanari, C., and Novaro, V. (2017). AKT1 and AKT2 isoforms play distinct roles during breast cancer progression through the regulation of specific downstream proteins. Sci. Rep. *7*, 44244–44312. https://doi.org/10.1038/srep44244.

35. Zhou, G.-L., Tucker, D.F., Bae, S.S., Bhatheja, K., Birnbaum, M.J., and Field, J. (2006). Opposing roles for Akt1 and Akt2 in Rac/Pak signaling and cell migration. J. Biol. Chem. *281*, 36443–36453. https://doi.org/10.1074/jbc.M600788200.

36. Bellacosa, A., De Feo, D., Godwin, A.K., Bell, D.W., Cheng, J.Q., Altomare, D.A., Wan, M., Dubeau, L., Scambia, G., Masciullo, V., et al. (1995). Molecular alterations of the AKT2 oncogene in ovarian and breast carcinomas. Int. J. Cancer *64*, 280–285. https://doi.org/10.1002/ijc.2910640412.

37. Parsons, D.W., Wang, T.-L., Samuels, Y., Bardelli, A., Cummins, J.M., DeLong, L.,

Silliman, N., Ptak, J., Szabo, S., Willson, J.K.V., et al. (2005). Mutations in a signalling pathway. Nature *436*, 792. https://doi.org/10.1038/436792a.

38. Dittmer, T.A., and Misteli, T. (2011). The lamin protein family. Genome Biol. *12*, 222–314. https://doi.org/10.1186/gb-2011-12-5-222.

39. Ho, C.Y., and Lammerding, J. (2012). Lamins at a glance. J. Cell Sci. *125*, 2087–2093. https://doi.org/10.1242/jcs.087288.

40. Lin, F., and Worman, H.J. (1993). Structural organization of the human gene encoding nuclear lamin A and nuclear lamin C. J. Biol. Chem. *268*, 16321–16326. https://doi.org/10.1016/S0021-9258(19)85424-8.

41. Peter, M., Kitten, G.T., Lehner, C.F., Vorburger, K., Bailer, S.M., Maridor, G., and Nigg, E.A. (1989). Cloning and sequencing of cDNA clones encoding chicken lamins A and B1 and comparison of the primary structures of vertebrate A-and B-type lamins. J. Mol. Biol. *208*, 393–404. https://doi.org/10.1016/0022-2836(89)90504-4.

42. Chu, C.-T., Chen, Y.-H., Chiu, W.-T., and Chen, H.-C. (2021). Tyrosine phosphorylation of lamin A by Src promotes disassembly of nuclear lamina in interphase. Life Sci. Alliance *4*, e202101120. https://doi.org/10.26508/lsa.202101120.

43. Heald, R., and McKeon, F. (1990). Mutations of phosphorylation sites in lamin A that prevent nuclear lamina disassembly in mitosis. Cell *61*, 579–589. https://doi.org/10.1016/0092-8674(90)90470-Y.

44. Kochin, V., Shimi, T., Torvaldson, E., Adam, S.A., Goldman, A., Pack, C.-G., Melo-Cardenas, J., Imanishi, S.Y., Goldman, R.D., and Eriksson, J.E. (2014). Interphase phosphorylation of lamin A. J. Cell Sci. *127*, 2683–2696. https://doi.org/10.1242/jcs.141820.

45. Peter, M., Nakagawa, J., Dorée, M., Labbé, J.C., and Nigg, E.A. (1990). In vitro disassembly of the nuclear lamina and M phase-specific phosphorylation of lamins by cdc2 kinase. Cell *61*, 591–602. https://doi.org/10.1016/0092-8674(90)90471-P.

46. Torvaldson, E., Kochin, V., and Eriksson, J.E. (2015). Phosphorylation of lamins determine their structural properties and signaling functions. Nucleus *6*, 166–171. https://doi.org/10.1080/19491034.2015.1017167.

47. Machowska, M., Piekarowicz, K., and Rzepecki, R. (2015). Regulation of lamin properties and functions: does phosphorylation do it all? Open Biol. *5*, 150094–215909. https://doi.org/10.1098/rsob.150094.

48. Simon, D.N., and Wilson, K.L. (2013). Partners and post-translational modifications of nuclear lamins. Chromosoma *122*, 13–31. https://doi.org/10.1007/s00412-013-0399-8.

49. Karoutas, A., Szymanski, W., Rausch, T., Guhathakurta, S., Rog-Zielinska, E.A., Peyronnet, R., Seyfferth, J., Chen, H.-R., de Leeuw, R., Herquel, B., et al. (2019). The NSL complex maintains nuclear architecture stability via lamin A/C acetylation. Nat. Cell Biol. *21*, 1248–1260. https://doi.org/10.1038/s41556-019-0397-z.

50. Zhang, Y.-Q., and Sarge, K.D. (2008). Sumoylation regulates lamin A function and is lost in lamin A mutants associated with familial cardiomyopathies. J. Cell Biol. *182*, 35–39. https://doi.org/10.1083/jcb.200712124.

51. Chow, K.-H., Factor, R.E., and Ullman, K.S. (2012). The nuclear envelope environment and its cancer connections. Nat. Rev. Cancer *12*, 196–209. https://doi.org/10.1038/nrc3219.

52. Capell, B.C., and Collins, F.S. (2006). Human laminopathies: nuclei gone genetically awry. Nat. Rev. Genet. *7*, 940–952. https://doi.org/10.1038/nrg1906.

53. Kang, S.-m., Yoon, M.-H., and Park, B.-J. (2018). Laminopathies; Mutations on single gene and various human genetic diseases. BMB Rep. *51*, 327–337. https://doi.org/10.5483/BMBRep.2018.51.7.113.

54. Worman, H.J., and Bonne, G. (2007). "Laminopathies": a wide spectrum of human diseases. Exp. Cell Res. *313*, 2121–2133. https://doi.org/10.1016/j.yexcr.2007.03.028.

55. Bell, E.S., Shah, P., Zuela-Sopilniak, N., Kim, D., Varlet, A.-A., Morival, J.L.P., McGregor, A.L., Isermann, P., Davidson, P.M., Elacqua, J.J., et al. (2022). Low lamin A levels enhance confined cell migration and metastatic capacity in breast cancer. Oncogene *41*, 4211–4230. https://doi.org/10.1038/s41388-022-02420-9.

56. Pajerowski, J.D., Dahl, K.N., Zhong, F.L., Sammak, P.J., and Discher, D.E. (2007). Physical plasticity of the nucleus in stem cell differentiation. Proc. Natl. Acad. Sci. USA *104*, 15619–15624. https://doi.org/10.1073/pnas.0702576104.

57. Cobb, A.M., Larrieu, D., Warren, D.T., Liu, Y., Srivastava, S., Smith, A.J.O., Bowater, R.P., Jackson, S.P., and Shanahan, C.M. (2016). Prelamin A impairs 53 BP 1 nuclear entry by mislocalizing NUP 153 and disrupting the Ran gradient. Aging Cell *15*, 1039–1050. https://doi.org/10.1111/acel.12506.

58. Gibbs-Seymour, I., Markiewicz, E., Bekker-Jensen, S., Mailand, N., and Hutchison, C.J. (2015). Lamin A/C-dependent interaction with 53 BP 1 promotes cellular responses to DNA damage. Aging Cell *14*, 162–169. https://doi.org/10.1111/acel.12258.

59. Gonzalez-Suarez, I., Redwood, A.B., Perkins, S.M., Vermolen, B., Lichtensztejin, D., Grotsky, D.A., Morgado-Palacin, L., Gapud, E.J., Sleckman, B.P., Sullivan, T., et al. (2009). Novel roles for A-type lamins in telomere biology and the DNA damage response pathway. EMBO J. *28*, 2414–2427. https://doi.org/10.1038/emboj.2009.196.

60. Liu, G.-H., Barkho, B.Z., Ruiz, S., Diep, D., Qu, J., Yang, S.-L., Panopoulos, A.D., Suzuki, K., Kurian, L., Walsh, C., et al. (2011). Recapitulation of premature ageing with iPSCs from Hutchinson–Gilford progeria syndrome. Nature *472*, 221–225. https://doi.org/10.1038/nature09879.

61. Manju, K., Muralikrishna, B., and Parnaik, V.K. (2006). Expression of disease-causing lamin A mutants impairs the formation of DNA repair foci. J. Cell Sci. *119*, 2704–2714. https://doi.org/10.1242/jcs.03009.

62. Muralikrishna, B., Chaturvedi, P., Sinha, K., and Parnaik, V.K. (2012). Lamin misexpression upregulates three distinct ubiquitin ligase systems that degrade ATR kinase in HeLa cells. Mol. Cell. Biochem. *365*, 323–332. https://doi.org/10.1007/s11010-012-1272-4.

63. Redwood, A.B., Perkins, S.M., Vanderwaal, R.P., Feng, Z., Biehl, K.J., Gonzalez-Suarez, I., Morgado-Palacin, L., Shi, W., Sage, J., Roti-Roti, J.L., et al. (2011). A dual role for A-type lamins in DNA double-strand break repair. Cell Cycle *10*, 2549–2560. https://doi.org/10.4161/cc.10.15.16531.

64. Zhang, Y., Wang, J., Huang, W., Cai, J., Ba, J., Wang, Y., Ke, Q., Huang, Y., Liu, X., Qiu, Y., et al. (2018). Nuclear Nestin deficiency drives tumor senescence via lamin A/C-dependent nuclear deformation. Nat. Commun. *9*, 3613–3614. https://doi.org/10.1038/s41467-018-05808-y.

65. Kim, B.N., Ahn, D.H., Kang, N., Yeo, C.D., Kim, Y.K., Lee, K.Y., Kim, T.-J., Lee, S.H., Park, M.S., Yim, H.W., et al. (2020). TGF-β induced EMT and stemness characteristics are associated with epigenetic regulation in lung cancer. Sci. Rep. *10*, 10597–10611. https://doi.org/10.1038/s41598-020-67325-7.

66. Tirino, V., Camerlingo, R., Bifulco, K., Irollo, E., Montella, R., Paino, F., Sessa, G., Carriero, M.V., Normanno, N., Rocco, G., and Pirozzi, G. (2013). TGF-β1 exposure induces epithelial to mesenchymal transition both in CSCs and non-CSCs of the A549 cell line, leading to an increase of migration ability in the CD133+ A549 cell fraction. Cell Death Dis. *4*, 620. https://doi.org/10.1038/cddis.2013.144.

67. Zhang, Y., Handley, D., Kaplan, T., Yu, H., Bais, A.S., Richards, T., Pandit, K.V., Zeng, Q., Benos, P.V., Friedman, N., et al. (2011). High throughput determination of TGFβ1/SMAD3 targets in A549 lung epithelial cells. PLoS One *6*, 20319–20330. https://doi.org/10.1371/journal.pone.0020319.

68. Chi, Y.-H., Wang, W.-P., Hung, M.-C., Liou, G.-G., Wang, J.-Y., and Chao, P.-H.G. (2022). Deformation of the nucleus by TGFβ1 via the remodeling of nuclear envelope and histone isoforms. Epigenet. Chromatin *15*, 1–17. https://doi.org/10.1186/s13072-021-00434-3.

69. Li, R.-H., Chen, M., Liu, J., Shao, C.-C., Guo, C.-P., Wei, X.-L., Li, Y.-C., Huang, W.-H., and Zhang, G.-J. (2018). Long noncoding RNA ATB promotes the epithelial– mesenchymal transition by upregulating the miR-200c/Twist1 axe and predicts poor prognosis in

breast cancer. Cell Death Dis. *9*, 1171–1187. https://doi.org/10.1038/s41419-018-1210-9.

70. Liu, M., Quek, L.-E., Sultani, G., and Turner, N. (2016). Epithelial-mesenchymal transition induction is associated with augmented glucose uptake and lactate production in pancreatic ductal adenocarcinoma. Cancer Metabol. *4*, 19. https://doi.org/10.1186/s40170-016-0160-x.

71. Sun, Y., Daemen, A., Hatzivassiliou, G., Arnott, D., Wilson, C., Zhuang, G., Gao, M., Liu, P., Boudreau, A., Johnson, L., and Settleman, J. (2014). Metabolic and transcriptional profiling reveals pyruvate dehydrogenase kinase 4 as a mediator of epithelial-mesenchymal transition and drug resistance in tumor cells. Cancer Metabol. *2*, 20. https://doi.org/10.1186/2049-3002-2-20.

72. Holaska, J.M. (2008). Emerin and the nuclear lamina in muscle and cardiac disease. Circ. Res. *103*, 16–23. https://doi.org/10.1161/CIRCRESAHA.108.172197.

73. Sullivan, T., Escalante-Alcalde, D., Bhatt, H., Anver, M., Bhat, N., Nagashima, K., Stewart, C.L., and Burke, B. (1999). Loss of A-type lamin expression compromises nuclear envelope integrity leading to muscular dystrophy. J. Cell Biol. *147*, 913–920. https://doi.org/10.1083/jcb.147.5.913.

74. Zhang, Y.E. (2009). Non-Smad pathways in TGF-β signaling. Cell Res. *19*, 128–139. https://doi.org/10.1038/cr.2008.328.

75. Jinnin, M., Ihn, H., and Tamaki, K. (2006). Characterization of SIS3, a novel specific inhibitor of Smad3, and its effect on transforming growth factor-β1-induced extracellular matrix expression. Mol. Pharmacol. *69*, 597–607. https://doi.org/10.1124/mol.105.017483.

76. Kalukula, Y., Stephens, A.D., Lammerding, J., and Gabriele, S. (2022). Mechanics and functional consequences of nuclear deformations. Nat. Rev. Mol. Cell Biol. *23*, 583–602. https://doi.org/10.1038/s41580-022-00480-z.

77. Stephens, A.D., Liu, P.Z., Banigan, E.J., Almassalha, L.M., Backman, V., Adam, S.A., Goldman, R.D., and Marko, J.F. (2018). Chromatin histone modifications and rigidity affect nuclear morphology independent of lamins. Mol. Biol. Cell *29*, 220–233. https://doi.org/10.1091/mbc.E17-06-0410.

78. Takaki, T., Montagner, M., Serres, M.P., Le Berre, M., Russell, M., Collinson, L., Szuhai, K., Howell, M., Boulton, S.J., Sahai, E., and Petronczki, M. (2017). Actomyosin drives cancer cell nuclear dysmorphia and threatens genome stability. Nat. Commun. *8*, 16013. https://doi.org/10.1038/ncomms16013.

79. Moustakas, A., and Stournaras, C. (1999). Regulation of actin organisation by TGF-beta in H-ras-transformed fibroblasts. J. Cell Sci. *112*, 1169–1179. https://doi.org/10.1242/jcs.112.8.1169.

80. Tam, W.L., and Weinberg, R.A. (2013). The epigenetics of epithelial-mesenchymal plasticity in cancer. Nat. Med. *19*, 1438–1449. https://doi.org/10.1038/nm.3336.

81. Kassianidou, E., Hughes, J.H., and Kumar, S. (2017). Activation of ROCK and MLCK tunes regional stress fiber formation and mechanics via preferential myosin light chain phosphorylation. Mol. Biol. Cell *28*, 3832–3843. https://doi.org/10.1091/mbc.e17-06-0401.

82. Liu, L., Zhou, W., Cheng, C.-T., Ren, X., Somlo, G., Fong, M.Y., Chin, A.R., Li, H., Yu, Y., Xu, Y., et al. (2014). TGFβ induces "BRCAness" and sensitivity to PARP inhibition in breast cancer by regulating DNA-repair genes. Mol. Cancer Res. *12*, 1597–1609. https://doi.org/10.1158/1541-7786.MCR-14-0201.

83. Pal, D., Pertot, A., Shirole, N.H., Yao, Z., Anaparthy, N., Garvin, T., Cox, H., Chang, K., Rollins, F., Kendall, J., et al. (2017). TGF-β reduces DNA ds-break repair mechanisms to heighten genetic diversity and adaptability of CD44+/CD24− cancer cells. Elife *6*, 21615–21642. https://doi.org/10.7554/eLife.21615.

84. Dellaire, G., and Bazett-Jones, D.P. (2004). PML nuclear bodies: dynamic sensors of DNA damage and cellular stress. Bioessays *26*, 963–977. https://doi.org/10.1002/bies.20089.

85. Podhorecka, M., Skladanowski, A., and Bozko, P. (2010). H2AX phosphorylation: its role in DNA damage response and cancer therapy. J. Nucleic Acids *2010*, 920161–920169. https://doi.org/10.4061/2010/920161.

86. Kanamoto, T., Hellman, U., Heldin, C.H., and Souchelnytskyi, S. (2002). Functional proteomics of transforming growth factor-β1-stimulated Mv1Lu epithelial cells: Rad51 as a target of TGFβ1-dependent regulation of DNA repair. EMBO J. *21*, 1219–1230. https://doi.org/10.1093/emboj/21.5.1219.

87. Kumar, A., Mazzanti, M., Mistrik, M., Kosar, M., Beznoussenko, G.V., Mironov, A.A., Garrè, M., Parazzoli, D., Shivashankar, G.V., Scita, G., et al. (2014). ATR mediates a checkpoint at the nuclear envelope in response to mechanical stress. Cell *158*, 633–646. https://doi.org/10.1016/j.cell.2014.05.046.

88. Cliby, W.A., Roberts, C.J., Cimprich, K.A., Stringer, C.M., Lamb, J.R., Schreiber, S.L., and Friend, S.H. (1998). Overexpression of a kinase-inactive ATR protein causes sensitivity to DNA-damaging agents and defects in cell cycle checkpoints. EMBO J. *17*, 159–169. https://doi.org/10.1093/emboj/17.1.159.

89. Nakamura, K., Sakai, W., Kawamoto, T., Bree, R.T., Lowndes, N.F., Takeda, S., and Taniguchi, Y. (2006). Genetic dissection of vertebrate 53BP1: a major role in non-homologous end joining of DNA double strand breaks. DNA Repair *5*, 741–749. https://doi.org/10.1016/j.dnarep.2006.03.008.

90. Rappold, I., Iwabuchi, K., Date, T., and Chen, J. (2001). Tumor suppressor p53 binding protein 1 (53BP1) is involved in DNA damage–signaling pathways. J. Cell Biol. *153*, 613–620. https://doi.org/10.1083/jcb.153.3.613.

91. Hatch, E.M., and Hetzer, M.W. (2016). Nuclear envelope rupture is induced by actin-based nucleus confinement. J. Cell Biol. *215*, 27–36. https://doi.org/10.1083/jcb.201603053.

92. Shi, L., Wen, H., and Shi, X. (2017). The histone variant H3. 3 in transcriptional regulation and human disease. J. Mol. Biol. *429*, 1934–1945. https://doi.org/10.1016/j.jmb.2016.11.019.

93. Guelen, L., Pagie, L., Brasset, E., Meuleman, W., Faza, M.B., Talhout, W., Eussen, B.H., De Klein, A., Wessels, L., De Laat, W., and van Steensel, B. (2008). Domain organization of human chromosomes revealed by mapping of nuclear lamina interactions. Nature *453*, 948–951. https://doi.org/10.1038/nature06947.

94. Van Steensel, B., and Belmont, A.S. (2017). Lamina-associated domains: links with chromosome architecture, heterochromatin, and gene repression. Cell *169*, 780–791. https://doi.org/10.1016/j.cell.2017.04.022.

95. Schreiner, S.M., Koo, P.K., Zhao, Y., Mochrie, S.G.J., and King, M.C. (2015). The tethering of chromatin to the nuclear envelope supports nuclear mechanics. Nat. Commun. *6*, 7159–7162. https://doi.org/10.1038/ncomms8159.

96. Hsia, C.-R., McAllister, J., Hasan, O., Judd, J., Lee, S., Agrawal, R., Chang, C.-Y., Soloway, P., and Lammerding, J. (2022). Confined migration induces heterochromatin formation and alters chromatin accessibility. iScience *25*, 104978–105001. https://doi.org/10.1016/j.isci.2022.104978.

97. Versaevel, M., Grevesse, T., and Gabriele, S. (2012). Spatial coordination between cell and nuclear shape within micropatterned endothelial cells. Nat. Commun. *3*, 671–682. https://doi.org/10.1038/ncomms1668.

98. Conery, A.R., Cao, Y., Thompson, E.A., Townsend, C.M., Ko, T.C., and Luo, K. (2004). Akt interacts directly with Smad3 to regulate the sensitivity to TGF-β-induced apoptosis. Nat. Cell Biol. *6*, 366–372. https://doi.org/10.1038/ncb1117.

99. Suwanabol, P.A., Seedial, S.M., Zhang, F., Shi, X., Si, Y., Liu, B., and Kent, K.C. (2012). TGF-β and Smad3 modulate PI3K/Akt signaling pathway in vascular smooth muscle cells. Am. J. Physiol. Heart Circ. Physiol. *302*, 2211–2219. https://doi.org/10.1152/ajpheart.00966.2011.

100. Van Berlo, J.H., Voncken, J.W., Kubben, N., Broers, J.L.V., Duisters, R., van Leeuwen, R.E.W., Crijns, H.J.G.M., Ramaekers, F.C.S.,

Hutchison, C.J., and Pinto, Y.M. (2005). A-type lamins are essential for TGF-β1 induced PP2A to dephosphorylate transcription factors. Hum. Mol. Genet. *14*, 2839–2849. https://doi.org/10.1093/hmg/ddi316.

101. Cenni, V., Bavelloni, A., Beretti, F., Tagliavini, F., Manzoli, L., Lattanzi, G., Maraldi, N.M., Cocco, L., and Marmiroli, S. (2011). Ankrd2/ARPP is a novel Akt2 specific substrate and regulates myogenic differentiation upon cellular exposure to H2O2. Mol. Biol. Cell *22*, 2946–2956. https://doi.org/10.1091/mbc.e10-11-0928.

102. Chin, Y.R., and Toker, A. (2010). The actin-bundling protein palladin is an Akt1-specific substrate that regulates breast cancer cell migration. Mol. Cell *38*, 333–344. https://doi.org/10.1016/j.molcel.2010.02.031.

103. Sanidas, I., Polytarchou, C., Hatziapostolou, M., Ezell, S.A., Kottakis, F., Hu, L., Guo, A., Xie, J., Comb, M.J., Iliopoulos, D., and Tsichlis, P.N. (2014). Phosphoproteomics screen reveals akt isoform-specific signals linking RNA processing to lung cancer. Mol. Cell *53*, 577–590. https://doi.org/10.1016/j.molcel.2013.12.018.

104. Kalousi, A., and Soutoglou, E. (2016). Nuclear compartmentalization of DNA repair. Curr. Opin. Genet. Dev. *37*, 148–157. https://doi.org/10.1016/j.gde.2016.05.013.

105. Gonzalez-Suarez, I., Redwood, A.B., Grotsky, D.A., Neumann, M.A., Cheng, E.H.Y., Stewart, C.L., Dusso, A., and Gonzalo, S. (2011). A new pathway that regulates 53BP1 stability implicates cathepsin L and vitamin D in DNA repair. EMBO J. *30*, 3383–3396. https://doi.org/10.1038/emboj.2011.225.

STAR★METHODS

KEY RESOURCES TABLE

REAGENT or RESOURCE	SOURCE	IDENTIFIER
Antibodies		
Mouse monoclonal anti-lamin A	Abcam	Cat#ab8980
Rabbit polyclonal anti-lamin A pS392	Abcam	Cat#ab58528
Rabbit polyclonal anti-lamin B1	Abcam	Cat#ab155319
Rabbit polyclonal anti-N-cadherin	Abcam	Cat#ab18203
Rabbit polyclonal anti-lamin A/C antibody	GeneTex	N/A
Rabbit polyclonal anti-lamin A pS22	Cell Signaling Technology	Cat#2026S
Rabbit polyclonal anti-AKT1 pS473	Cell Signaling Technology	Cat#9271S
Rabbit monoclonal anti-AKT2 (clone D6G4)	Cell Signaling Technology	Cat#3063S
Rabbit monoclonal anti-AKT2 pS474 (clone D3H2)	Cell Signaling Technology	Cat#8599S
Rabbit polyclonal anti-ATR	Cell Signaling Technology	Cat#2790
Rabbit polyclonal anti-ERK pT202/pY204	Cell Signaling Technology	Cat#9101
Rabbit polyclonal anti-emerin	Santa Cruz Biotechnology	Cat#sc-15378
Mouse monoclonal anti-Slug (clone A-7)	Santa Cruz Biotechnology	Cat#sc-166476
Rabbit polyclonal anti-Twist	Santa Cruz Biotechnology	Cat#sc-15393
Mouse monoclonal anti-AKT1 (clone B-1)	Santa Cruz Biotechnology	Cat#sc-5298
Mouse monoclonal anti-Smad2/3 (clone C-8)	Santa Cruz Biotechnology	Cat#sc-133098
Mouse monoclonal PML (clone PG-M3)	Santa Cruz Biotechnology	Cat#sc-966
Mouse monoclonal anti-His Tag (clone H-3)	Santa Cruz Biotechnology	Cat#sc-8036
Rabbit polyclonal and anti-ERK	Santa Cruz Biotechnology	Cat#sc-94
Mouse monoclonal anti-FLAG (clone M2)	Sigma-Aldrich	Cat#F1804
Mouse monoclonal anti-vimentin (clone VIM-13.2)	Sigma-Aldrich	Cat#V5255
Rabbit polyclonal anti-fibronectin	Sigma-Aldrich	Cat#F3648
Mouse monoclonal anti-actin (clone AC-15)	Sigma-Aldrich	Cat#A1978
Mouse monoclonal anti-αtubulin (DM1A)	Sigma-Aldrich	Cat#T6199
Rabbit polyclonal anti-lamin A pS390	Merck Millipore	Cat#ABT1388
Rabbit polyclonal anti-lamin A pS404	Merck Millipore	Cat#ABT1387
Rabbit polyclonal anti-H3K27me3	Merck Millipore	Cat#07449
Mouse monoclonal anti-H2AX pS139 (clone JBW301)	Merck Millipore	Cat#05-636
Mouse monoclonal anti-E-cadherin (clone 36)	BD Biosciences.	Cat#610182
Mouse monoclonal anti-53BP1 (clone 19)	BD Biosciences.	Cat#612522
Mouse monoclonal anti-HA antibody	Biolegend	Cat#MMS-101P
Rabbit polyclonal anti-Smad3 pS423/425	Invitrogen	Cat#44-246G
Chemicals, peptides, and recombinant proteins		
phalloidin (conjugated with Alexa Fluor-546)	Invitrogen	Cat#R415
Recombinant human TGFβ	R&D Systems	Cat#240-B-002
Active recombinant human AKT1	Merck Millipore	Cat#14-453
Active recombinant human AKT2	Merck Millipore	Cat#14-339
MK2206	Selleckchem	Cat#S1078

(*Continued on next page*)

Continued

REAGENT or RESOURCE	SOURCE	IDENTIFIER
LY294002	Selleckchem	Cat#S1105
DZNep	Selleckchem	Cat#S7120
PD98059	Cell Signaling Technology	Cat#S1177
SP600125	Merck Millipore	Cat#420128
SB23580	Calbiochem	Cat#559389
Y27632	EMD Chemicals	Cat#688000
Cytochalasin D	Sigma-Aldrich	Cat#C8273
ML-7	Sigma-Aldrich	Cat#12764
Blebbistatin	Sigma-Aldrich	Cat#B0560
methylstat	Sigma-Aldrich	Cat#SML0343
SIS3	Santa Cruz Biotechnology.	Cat#sc-222318
Critical commercial assays		
Phos-Tag™ Phosphoprotein Gel Stain	ABP Biosciences.	Cat#P005A
Experimental models: Cell lines		
Human: A549	Dr. Sung-Liang Yu (National Taiwan University)	N/A
Human: PANC-1	Dr. Sung-Liang Yu (National Taiwan University)	N/A
Human: NCI-H358	Dr. Sung-Liang Yu (National Taiwan University)	N/A
Human: MCF7	Yeun-Ting Hsieh (Taichung Veterans General Hospital)	N/A
Human: Huh7	Dr. Ya-Hui Chi (National Health Research Institutes)	N/A
Human: HEK293T	ATCC	CRL-3216
Recombinant DNA		
Plasmid: HA-Smad2	Addgene	Cat#11734
Plasmid: FLAG-Smad3	Addgene	Cat#11742
Plasmid: HA-AKT2	Addgene	Cat#16000
Plasmid: HA-AKT1	Dr. Chi-Ying Huang (National Yang Ming Chiao Tung University)	N/A
Plasmid: FLAG-lamin A	This paper	N/A
Plasmid: pMD.G	National RNAi Core Facility (Academia Sinica)	https://rnai.genmed.sinica.edu.tw/vector.html
Plasmid: pCMV-ΔR8.91	National RNAi Core Facility (Academia Sinica)	https://rnai.genmed.sinica.edu.tw/vector.html
Plasmid: pLKO-AS1-puro	National RNAi Core Facility (Academia Sinica)	https://rnai.genmed.sinica.edu.tw/vector.html
Software and algorithms		
ZEN2 software	Carl Zeiss	N/A
Odyssey® CLx Imaging System	LI-COR Biosciences	N/A
Image J	NIH	https://imagej.nih.gov/ij/
EXCEL	Microsoft	N/A
GraphPad Prism	GraphPad	https://www.graphpad.com/features
Photoshop CS6	Adobe	N/A
Illustrator CS6	Adobe	N/A

RESOURCE AVAILABILITY

Lead contact

Further information on resources and reagents should be directed to the lead contact, Dr. Hong-Chen Chen (hcchen1029@nycu.edu.tw).

Materials availability

Materials generated in this study are available from the lead contact, Dr. Hong-Chen Chen (hcchen1029@nycu.edu.tw).

Data and code availability

- All data will be shared upon reasonable request by the lead contact, Dr. Hong-Chen Chen (hcchen1029@nycu.edu.tw).
- This paper does not report any original code.
- Any additional information required to reanalyze the data reported in this paper is available from the lead contact upon request.

EXPERIMENTAL MODEL AND SUBJECT DETAILS

Cell culture, treatment and transfection

A549 (human lung carcinoma) cells were cultured in RPMI1640 medium supplemented with 10% FBS and antibiotics. HEK293T (human embryonic kidney cells), Huh7 (human hepatoma), MCF-7 (human mammary adenocarcinoma), PANC-1 (human pancreatic carcinoma) and NCI-H358 (human lung carcinoma) cells were cultured in DMEM medium supplemented with 10% FBS and antibiotics. Cells were incubated in humidified conditions at 37°C and 5% CO2 and passaged before exceeding 90% confluency. TGFβ (5 ng/ml) and MK2206 (5 μM) were used to treat cells for indicated time in the figures. Transient transfection was performed using Lipofectamine 2000 (Invitrogen).

METHOD DETAILS

Plasmids

For FLAG-lamin A, the human lamin A cDNA was cloned into the pCMV-3Tag-3A plasmid using BamHI and XhoI sites. The mutagenesis of FLAG-lamin A S22A, S390A, S392A or S404A was performed using the Quikchange site-directed mutagenesis kit (Stratagene) and the desired mutations were confirmed by the dideoxy DNA sequencing. HA-AKT1 was kindly provided by Dr. Chi-Ying Huang (National Yang Ming Chiao Tung University). HA-AKT2 (16000) HA-Smad2 (11734), and FLAG-Smad3 (11742) were purchased from Addgene.

Lentivirus-mediated gene knockdown

The lentiviral expression system was obtained from the National RNAi Core Facility (Academia Sinica, Taiwan). The target sequence for AKT1 was 5′- GGACAAGGACGGGCACATTAA-3′. The target sequence for AKT2 was 5′- CGGCTCCTTCATTGGGTACAA-3′. The target sequence for Smad2 was 5′- CCTAA GTGATAGTGCAATCTT-3′. The target sequence for Smad3 was 5′- GAGCCTGGTCAAGAAACTCAA-3′. The target sequence for luciferase was 5′-GCGGTTGCCAAGAGGTTCCAT-3′ For the lentivirus production, HEK293T cells were co-transfected with 0.25 μg pMD.G, 2.25 μg pCMV-ΔR8.91, and 2.5 μg pLKO-AS1-puro-shRNA through Lipofectamine 2000. After three days, the medium with the viral particles was collected and stored at −80°C. Cells were infected by lentiviruses for 24 h and subsequently selected with puromycin (2 μg/mL) for 5 days before further analysis.

Immunofluorescence staining, microscopy, and image analysis

Cells were fixed with phosphate-buffered saline containing 4% paraformaldehyde (for 15 min), excepting that for the staining of ATR, cells were fixed with 100% methanol (at -20°C for 10 min). Cells were permeabilized with 0.1% Triton X-100 (for 60 min) or 0.5% Triton X-100 (for 20 min) after methanol- or paraformaldehyde-fixation, respectively. The fixed cells were stained with primary antibodies for 1 h and then incubated with Alexa Fluor 488- or 546-conjugated secondary antibodies or phalloidin for 1 h. Cells were mounted on the slides with mounting medium (Anti-Fade Dapi-Fluoromount-G, Southern Biotech). The images (2048x2048 pixels) were acquired using an upright fluorescence microscope (Axio imager, M2 Apotome2 system, Carl Zeiss), which was equipped with 63x and 100x oil-immersion objective lens (1.4 NA, Plan Apochromat) and a camera (ORCA-Flash4.0 V2; Hamamatsu). For Figure S8, images were acquired by a Carl Zeiss LSM880 confocal microscope imaging system with a Zeiss Plan-Apochromat 63x/NA 1.4 oil immersion objective. The representative images were cropped by Photoshop CS6 (Adobe) and assembled by Illustrator CS6 (Adobe).

Measurement of nuclear deformation and circularity

The cells were fixed and stained for lamin A and DNA. The immunofluorescence images of nuclei were taken by a microscope (Axio imager, M2 Apotome2 system, Carl Zeiss) with the 100x oil-immersion objective, and quantitated by the ZEN2 software (Carl Zeiss). Our criteria for nuclear crumpling are (i) a nucleus has one concave with angle $\leq 160°$ and (ii) a nucleus has two or more concaves, all of which have an angle between 90° and 160°. Our criterion for nuclear lobulation is that a nucleus has two or more concaves, any of which has an angle $\leq 90°$. The formula of 4π x area/perimeter^2 was used to measure the nuclear circularity.

Live cell imaging

A549 cells were transiently transfected with the GFP-H2B plasmid and cultured in the presence or absence of TGFβ for 12 h. Cells were then incubated in a micro-cultivation system with temperature and CO_2control devices (Carl Zeiss). The cells were monitored on an inverted microscope (Axio Observer; Carl Zeiss) using an EC Plan-NEOFLUAR 40 × NA 0.75 objective. Images were captured every 10 min for 12 h using a digital camera (ORCA-Flash4.0 V2; Hamamatsu) and were processed by the ZEISS ZEN2 image software.

Immunoblotting and immunoprecipitation

To prepare whole-cell lysates, cells were lysed on ice in RIPA buffer (0.1% SDS, 1% sodium deoxycholate, 1% NP-40, 150 mM NaCl, 50 mM Tris-HCl, 1 mM EDTA, pH 7.4) and the protein concentration was measured using the Bradford protein assay reagent (Bio-Rad). For immunoprecipitation, cell lysates (200 μg) were incubated with anti-FLAG antibody (1 μg) and protein A-Sepharose beads (GE Healthcare) for 2 h at 4°C. The beads were washed with RIPA buffer for three times and resuspended in SDS sample buffer for immunoblotting analysis. For immunoblotting, samples were subjected to SDS-polyacrylamide gel electrophoresis and transferred to nitrocellulose membranes. Membranes were probed with indicated primary antibodies and subsequently with secondary antibodies conjugated to horseradish peroxidase or IR-780/680 iodide fluorescence dye, which were then scanned by the luminescence imaging system (LAS-4000; Fujifilm) or the Odyssey® CLx Imaging System (LI-COR Biosciences), respectively.

In vitro kinase assay

His-tagged lamin A proteins were expressed in*Escherichia coli* (BL21) and the bacterial pellets were lysed in extraction buffer (8 M Urea, 25 mM Tris, pH8.0 and 0.5 M NaCl) with pulsed sonication. The lysates were centrifuged (at 14,000 × g for 10 min at 4°C) and the supernatants were dialyzed with storage buffer (25 mM Tris, pH8.0, 0.5 M NaCl, and 1 mM DTT). Recombinant His-lamin A protein (2 μg) was incubated with 0.5 μg of active AKT1 (Merck Millipore, #14-453) or AKT2 (Merck Millipore, #14-339) in the kinase buffer (25 mM Tris, pH7.4, 20 mM $MgCl_2$ and 2 mM ATP) at 30°C for 20 min. The reaction was terminated by the SDS sample buffer and analyzed by the immunoblotting.

Cell migration assay

A549 cells were collected, suspended in serum-free medium and subjected to the Neuro Probe 48-well chemotaxis chamber (Cabin John, MD, USA). The lower chamber was loaded with serum-free medium with type I collagen (10 μg/mL), containing with or without TGFβ. The cells (1.25×10^4) in serum-free medium were added to the upper chamber. The lower and upper chambers were separated by a polycarbonate membrane (Poretics, Livermore, CA) with 5 μm pore size. The cells were allowed to migrate for 6 h at 37°C in a humidified atmosphere containing 5% CO_2. The membranes were fixed with methanol and stained with 10% Giemsa. The cells that migrated to the lower side of the membrane were counted under a light microscope.

QUANTIFICATION AND STATISTICAL ANALYSIS

Densitometric quantitation of the Immunoblotting images was performed using the NIH Image J software or Odyssey® CLx Imaging System (LI-COR Biosciences). The immunofluorescence images were quantitated by the ZEN2 software (Carl Zeiss). All values are presented as means ± SD, except in Figures 6B, 6C, S7A and S7B, the means ± SEM were presented for values. Data were obtained from three independent experiments, and the numbers of the cells counted in the experiments were described in figure legends. Data analysis was performed by Excel or GraphPad Prism. The two-tailed Student's *t*-test was used to determine whether the differences between experimental values were significant. $P < 0.05$ was considered statistically significant (*P<0.05, **P<0.01, ***P<0.001).